PROFESSOR MOHAMED SHAKER S. ADAM (Orcid ID : 0000-0001-8826-3558)

Article type : Article

Hybrid organic-inorganic Cu(II) iminoisonicotine@TiO_2@Fe_3O_4 heterostructure as efficient catalyst for cross-couplings

Mohamed Shaker S. Adam[1,2]* | Farman Ullah[3] | Mohamed M. Makhlouf[4,5]*

[1] Department of Chemistry, College of Science, King Faisal University, P.O. Box 380 Al Hofuf 31982 Al Ahsa, Saudi Arabia.
[2] Chemistry Department, Faculty of Science, Sohag University, Sohag-82534, Egypt.
[3] Department of Chemistry, Winnipeg University 515 Portage Avenue, Winnipeg, Manitoba, R3B 2E9 Canada.
[4] Department of Sciences and Technology, Rania University College, Taif University, Rania 12975, Saudi Arabia.
[5] Department of Physics, Damietta Cancer Institute, Damietta, 34517, Egypt.
*Correspondence E-mail: madam@kfu.edu.sa; shakeradam61@yahoo.com (M.S.S. Adam) and m_makhlof@hotmail.com (M.M. Makhlouf)

Abstract

Two novel mononuclear copper (II) complex catalysts were synthesized from a new tridentate iminoisonicotine ligand (HL) by coordination with Cu(II) ion, with (CuL@TiO_2@Fe_3O_4) and without (CuL) immobilization on TiO_2 coated nanoparticles of Fe_3O_4. The ester moiety on the back of the ligand was utilized for immobilization on nanoparticles of Fe_3O_4. Both ligand and CuL complex were fully characterized by alternative spectral techniques (nuclear magnetic resonance, infrared, ultraviolet-visible and mass spectroscopy, and elemental analyses). Different analytical techniques were used to identify the structural feature and morphology of the immobilized copper catalyst (CuL@TiO_2@Fe_3O_4) core-shell-shell system. The structural analysis revealed that the catalyst system is composed of both agglomerated nanospheres and deformed nanorods. Both copper catalysts, immobilized CuL@TiO_2@Fe_3O_4 and un-immobilized CuL were studied in heterogeneous and homogeneous catalysis, respectively, for Suzuki-Miyaura (C—C) and Buchwald-Hartwig (C—N) cross-coupling reactions of various heteroaryl halides. Both catalysts showed good catalytic potential under the controlled optimal reaction conditions. In contrast to the homogeneous catalyst (CuL), the heterogeneous catalyst (CuL@TiO_2@Fe_3O_4) showed slightly better catalytic performance. The characteristic obtains supported the catalytic potential of the current samples. Reusability/recycling of both catalysts was also investigated in C—C cross-coupling reactions. It was found that the homogeneous catalyst (CuL) could be only recycled up to 3 times, whereas the heterogeneous one (CuL@TiO_2@Fe_3O_4) could be reused up to 7 times with good efficiency.

1 | INTRODUCTION

Enormous organic syntheses catalyzed by metals, as homogeneous metal-chelates[1] or heterogeneous metal-oxides,[2,3] are extensively developed, which are pivotal in the industrial application.[4] The vast catalytic applications of various metal species, as metal ion chelates, are limited only to the homogeneous phase, with coagulating features and non-recyclability.[5] The immobilized metal nanoparticles on the surface of supporting material are a spectacular way to enhance their catalytic sufficiency and reactivity. Moreover, the metal species agglomeration in the homogeneous phase could be reduced with alternative immobilization processes that could also increase their recyclability power in the catalytic systems. In most of the electrocatalysis[6-8] and cross-coupling reactions, the immobilized copper nanoparticles, as complexes, are of strong interest than the other high-cost transition metal nanoparticles, *e.g.* palladium and platinum. Consequently, there are many published works regarding various applications, of copper nanoparticles in catalysis, supported on SiO_2 coated Fe_2O_3 nanoparticles.[9-16]

C_{sp2}—C_{sp2} and C_{sp2}—N cross-coupling reactions are a facile approach to synthesize biaryls molecular collection,[17] which are highly valuable as intermediates for materials manufacturers in pharmaceutical and biochemical industries.[18] Many comprehensive studies reported various approaches to synthesize biaryl molecular collections from heteroaryl bromides and chlorides *via* C—C and C—N bond formation reaction utilizing various transition metal complexes as catalysts homogeneously or heterogeneously supported on various supporting reagent. The most well-known supporting materials are Fe_3O_4 nano-particles and Fe_3O_4 nano-particles coated by SiO_2, whereas Fe_3O_4 nanoparticles coated by TiO_2 are not enough studied for such cross-coupling reactions, however, it is well documented that TiO_2 coated Fe_2O_3 nano-spindles could be used for different proposes.[19,20] Indeed, titanium dioxide as an important example of viable support, like SiO_2, ZrO_2 and ZnO, which has gained much importance with specific characteristics such as cost-effectiveness, nontoxicity, good biological applicability and easy preparation.[21,22] The TiO_2 modified Fe_2O_3 nano-spindles are well documented for various applicable proposes,[21,22] *e.g.* in photochemistry and photocatalysis.[23-30]

Substituted imines (—CH=N—), are considered as the most active chelating ligands with many transition metal ions at different oxidation states giving high stable metal pincer chelates.[31,32] Copper (II)-imine complexes have appeared as flourished structures due to their widespread activities against a variety of targets,[33] including high corrosion inhibition,[34,35] photosynthetic inhibition,[36] DNA/RNA binding cleavage[37,38] and antioxidants.[39] Copper as a cheap 3d group element has alternative oxidation states and unequaled features in tuning the Cu nanoparticles size.[40,41] The electrochemical features of Cu(II)-chelates for the Cu(II)/Cu(I) the electron transfer couple[42] realized that many Cu(II)-complexes were applied as homogeneous and heterogeneous catalysts in alternative catalytic processes.[43-48] Vast and enormous applicability of metal-imine framework complexes are explored in wide areas, *e.g.* in the bio- and pharmaceutical industry,[49-52] sensors,[53] organic photovoltaics[54] and in catalysis.[55-58] C—C, C—S, C—O and C—N cross-coupling reactions in various organic syntheses are achieved by using imine complexes as catalysts.[59] To emphasize the organocatalysts immobilization on coated Fe_3O_4 could be enhanced with functional active reagents, as a linker, *e.g.* CPTMS (3-chlorooproрyltrimethoxysilane)[60] or APTES (3-aminopropyltriethoxysilane).[61,62] To save cost and reduce the number of synthetic steps for such immobilized metal complexes on Fe_3O_4-NPs, significant functional groups in the backbone of the coordinated ligands to the central metal ion of the catalyst could interact with Fe_3O_4-TiO_2 nanoparticles to be immobilized through those groups, e.g. —OH (hydroxyl group)[63,64] and —OR (alkoxy group).[65,66] The presence of such groups in the coordinated ligand could considerably support metal complexes on Fe_3O_4 and/or TiO_2.[67]

Building on those efforts, it is a motivation to design and synthesize novel copper (II) imine complex as a homogeneous (CuL) and heterogeneous (CuL@TiO_2@Fe_3O_4) catalysts for C—C and C—N cross-coupling systems. The ester moiety on the back of ligand could be a benefit for immobilization on Fe_3O_4 nanoparticles coated by TiO_2. A comparative study on the catalytic potential of these two Cu(II)-catalysts was examined under various reaction conditions. Additionally, the limit of the reusability of both catalysts was also examined.

2 | EXPERIMENTAL

2.1 | Materials and physical measurements

Starting materials, reagents and solvents used in this study are commercially available. The supplementary materials include a subsection listing of all chemicals, purchase companies, purity grades and their melting or boiling points (**Table S1**). Elemental analyses of the samples were measured by GMBH varioEI model V2.3 of the CHN machine at room temperature. Nuclear magnetic resonating spectroscopy was measured by Bruker ARX400 as FT-NMR multinuclear spectrometric machine at 25 °C using 400.1 MHz for hydrogen nuclei and 100.6 MHz for carbon nuclei. Melting point and the decomposition temperatures of the prepared copper chelating complex and its coordinated ligand were estimated using a Gallenkamp (Sanyo) machine. Magnetic features of the studied copper complex were evaluated on magnetic susceptibility balance (Sherwood Scientific, Cambridge, UK). The IR spectra of the prepared samples were measured with an FT-IR spectrophotometer (Agilent Technologies Cary 630 FT-IR spectrophotometer). IR spectra were measured at room temperature over solid samples in 4000-400 cm^{-1}. Electronic transition spectra of the coordinated ligand and its corresponded Cu-complex were measured in UV-1800 SHIMADZU UV-spectrophotometer within a 10 mm matched quartz cell. Moreover, data were determined in λ_{max} (nm) in the region 190-800 nm using an aqueous solution at room temperature. Moreover, mass spectroscopy of CuL was recorded in m/z using waters Qtof Micro YA263 mass spectrometer at room temperature.

2.2 | Synthesis

2.2.1 Synthesis of (*E*)-ethyl-2-((2-methoxyethylimino)methyl)isonicotinate (HL)

Ligand (HL) was prepared according to the general Schiff base preparing procedure: ethyl 2-formylisonicotinate (1.30 g, 7.26 mmol) was treated with 2-methoxyethanamine (0.653 g, 8.72 mmol) in toluene (15 mL) provided orange red gummy solid of HL (Yield = 1.35g with 0.03 g error, 92%), Scheme 1.

^{1}H NMR (400.6 MHz, $CDCl_3$): δ = 8.72 (d, J = 3.6 Hz, 1H), 8.46 (s, 1H), 8.42 (s, 1H), 7.83 (m, 1H), 4.40 (q, ^2J = 7.2,^1J = 14.4 Hz, 2H), 3.85 (t, J = 5-1 Hz, 2H), 3.71 (t, J = 5-1, 2H), 3.33 (s, 3H), 1.38 ppm (t, J = 6.9Hz, 3H).

^{13}C NMR (100.1 MHz, $CDCl_3$): δ = 164.80, 162.75, 155.39, 150.1, 138.45, 123.76, 120.71, 71.78, 61.85, 60.85, 58.83 and 14.20 ppm.

FT-IR (KBr taplet, $\bar{\nu}$, cm^{-1}): 3066 ($C—H_{aromatic}$), 2919 ($C—H_{aliphatic}$), 1718 (C=O), 1682 ($CH=N_{Schiff\ base}$), 1625 ($CH=N_{pyridine}$), 1344 (C—O), 1208 ($C—O_{carboxlate}$) and 1110 cm^{-1} (C—N).

2.2.2 | Synthesis of Cu(II)-complex (CuL)

Copper chloride dihydrate (0.17 g, 1.0 mmol, in 10 mL water) was added dropwise to a methanolic solution of ligand (HL) (0.22 g, 1.0 mmol, in 10 mL methanol) at room temperature. The reaction mixture was heated at 80 °C for 1 h. The colour of the reaction mixture was slowly changed to dark green with the formation of precipitate upon cooling down to room temperature. The crude product of the complex was collected by filtration. The complex was purified by recrystallization in hot methanol awarding 77% (0.26 g with 0.04 g error) of CuL, Scheme 2.

FT-IR (KBr taplet, $\bar{\nu}$, cm^{-1}): 3056 ($C—H_{aromatic}$), 2925 ($C—H_{aliphatic}$), 1724 (C=O), 1611 ($CH=N_{Schiff\ base}$), 1559 ($CH=N_{pyridine}$), 1282 (C—O), 1211 ($C—O_{carboxlate}$), 1111 and 1017 cm^{-1} (C—N), 687 (Cu—O), 463 and 439 cm^{-1} (Cu—N).

2.2.3 | Synthesis of Fe_3O_4

The nanoparticles of Fe_3O_4 were prepared according to the reported method[25,26,68] by mixing $FeCl_2.4H_2O$ with $FeCl_3.6H_2O$ in a ratio of 2 : 1, respectively, in a mixture of water (98 mL) and EtOH (2 mL) in a Schlenk line. The mixed contents were kept with stirring for about a half-hour, then 20 mL of an aqueous NaOH (2.0 N) was added dropwisely to get a pH of the solution about 10–12. The reaction mixture was turned to dark brown colour upon pH 10-12. Then 0.3 mol of an aqueous solution of urea was slowly added to the reaction mixture, followed by stirring for 5 h at room temperature. The resulted mixture was kept for 30 min at 70 °C and then slowly cooled down to 25 °C. The mixture was centrifuged for a few minutes as a result of black precipitate. The black precipitate was collected by filtration and washed with H_2O and ethanol multiple times until pH became ≈ 7. The final nanoparticles of Fe_3O_4 were collected and dried in an oven at 40 °C for 3 h.

2.2.4 | Synthesis of $TiO_2@Fe_3O_4$

The preparation of $TiO_2@Fe_3O_4$ was carried out according to the reported method.[25,26,68] A solid Fe_3O_4 (0.05 g) was kept in a sonicated both in 20 mL of ethanol. In another beaker, 0.2 g of CTAB was dissolved in 15 mL of an aqueous media. The CTAB solution was added dropwisely to the suspended ethanolic solution of Fe_3O_4. After that TiO_2 (0.05 g) in isopropanol (8 mL) was added to the previous solution. The resulted reaction mixture was treated by ammonia until the pH of the reaction mixture was between 8 to 9 to afford a white gel. The final reaction mixture was stirred magnetically for almost 24 h at the ambient temperature to give a well uniform dispersed precipitate. The fine precipitate was extracted by filtration washed within water and ethanol. The final precipitate was dried in an oven at 60 °C awarding nanoparticles of paramagnetic $TiO_2@Fe_3O_4$.

2.2.5 | Immobilization of HL on $Fe_3O_4@TiO_2$

The solid-supported ligand ($HL@TiO_2@Fe_3O_4$) was prepared by mixing a solution of ligand (HL) 1.0 g in acetonitrile (20 mL) to a suspension of $TiO_2@Fe_3O_4$ in acetonitrile (20 mL), and then the mixture was stirred for 12 h at room temperature. The colour of the suspension of $TiO_2@Fe_3O_4$ was changed from dark-gray to dark brown. The final product was collected by filtration, washed with acetonitrile and then dried in an oven at 50 °C for 12 hours.

2.2.6 | Supporting of Cu^{2+} ions on $HL@TiO_2@Fe_3O_4$

$HL@TiO_2@Fe_3O_4$ (0.5 g) was suspended in acetonitrile (25 mL) and sonicated for 30 min. The sonication process was carried out with an ultrasonic bath (Elmasonic S150 - TEVOTECH) using ultrasound waves with frequencies of ~ 20 kHz. During sonication, the solution keeps on ice to stop heating up and degrading of the sample. Then, 0.5 g of copper chloride dihydrate in acetonitrile (15 mL) was added dropwise to the resulted suspended of $HL@TiO_2@Fe_3O_4$. The colour of the suspended $HL@TiO_2@Fe_3O_4$ was slowly changed from dark brown to dark green, which was left on stirring for 24 h at room temperature. The final product was collected by filtration, washed few times with acetonitrile and water then s dried in an oven at 50 °C for 12 h.

2.3 | Characterization of $CuL@TiO_2@Fe_3O_4$ nanoparticles

Fe_3O_4-nanoparticles, which coated by TiO_2 and $CuL@TiO_2$, were characterized by FT-IR spectra and with a VSM-9600 LDJ vibrating sample magnetometer with a 1T magnet. The phase morphology of the materials was investigated by XRD using a Brucker Axs-D8 Advance-diffractometer with Cu–K_a radiation at 0.154178 nm within a range of 2θ from 10.0 to 90.0 in a continual scan type. The elemental composition of the surface morphology of the TiO_2 and

$CuL@TiO_2$ coated Fe_3O_4-nanoparticles were measured by SEM, Model JEOL JSM 5410 machine using FE-SEM and with EDS (FE-SEM/EDS-Germany) detector (at 15 kV). TEM analyses (Transmission electron microscope machine-model: Jeol-1230) was applied with an acceleration voltage (200 kV) to evaluate the size of Fe_3O_4-nanoparticles, $TiO_2@Fe_3O_4$ and $CuL@TiO_2@Fe_3O_4$. The suspended material sizes in an aqueous media were measured with Cilas dual scattering particle size analyzer Nano DS. The Brunauer-Emmett-Teller (BET) specific surface area of the new nanoparticles of $CuL@TiO_2@Fe_3O_4$ was evaluated by nitrogen gas adsorption isotherms at 77.38 K within relative pressures range from 0.05 to 0.30 atm. Micrometrics ASAP2010 as a volumetric adsorption apparatus was used for the adsorption isotherm studies. Nanoparticles of $CuL@TiO_2@Fe_3O_4$ were investigated under degassed conditions at 40 °C for 20 h.

2.4 | Catalytic procedures

2.4.1 | C—C and C—N cross-coupling reaction

Homogeneous and heterogeneous cross-coupling reactions of Suzuki-Miyaura or Buchwald-Hartwig amination reactions were carried out in two-necked 50 mL round bottom flask with water circulation condenser. Loaded with phenylboronic acid (1.1 mmol) in 10 mL solvent (toluene, chloroform, ethanol, water and water-ethanol mixture), Cu(II)-complex (CuL, homogeneously, 0.01, 0.02, 0.05 and 0.1 mmol) or $CuL@TiO_2@Fe_3O_4$ (heterogeneously, 0.05, 0.1 or 0.2 and 0.5 g), and base 2.0 mmol (K_2CO_3, *t*BuOK, K_3PO_4 and KOH). The reaction was initiated by the addition of aryl halide (1.0 mmol) under the aerobic condition and the mixture was stirred under reflux conditions at 100 °C for given reaction time.

The progress of the reaction was monitored by Shimadzu Gas Chromatography mass spectrometer (GC-MS model QP2010 SE, Rxi-5 Sil MS capillary column (30 m length × 0.25 mm ID × 025 um film thickness). The sample was injected into the GC-MS at room temperature. The initial oven temperature was 40 °C and hold for 1 min. The temperature rate was increased with 10 °C min^{-1} up to 200 °C. The carrier gas was Helium with high purity up to 99.999%, which was applied with a flow rate of 1 mL/min. Lab solution software was used to analyze the percentages yields of the obtained products.

2.5 | Reusability of CuL homogeneously and heterogeneously

The recycling of homogeneous catalyst (CuL) at 0.02 mmol scale and heterogeneous catalyst (CuL@TiO_2@Fe_3O_4) at 0.05 g scale were investigated in C—C coupling reaction using optimized reaction condition (phenylboronic acid, 1.1 mmol, 2-pyridyl bromide, 1.0 mmol, K_2CO_3, 3.0 mmol, and toluene 10 mL, at 100 °C). The catalyst from homogeneous catalysis (CuL) was simply collected by filtration after cooling down to the room temperature and re-subjected in catalysis under the same reaction condition. While the heterogeneous catalyst (CuL@TiO_2@Fe_3O_4) was collected by a magnet from the reaction mixture, washed with toluene, dried in an oven and then re-subjected in the next trill under the same reaction condition.

3 | RESULTS AND DISCUSSION

3.1 | Synthesis and characterization of ligand (HL) and copper complex (CuL)

The novel neutral tridentate pincer ligand (HL) was prepared by using Schiff base general procedure from ethyl 2-formylisonicotinate and 2-methoxyethanamine in toluene provided HL in good yield (92%). The copper complex (CuL) was synthesized by the treatment of HL with $CuCl_2.2H_2O$ in methanol under mild condition afforded CuL in good yield (77%) (**Scheme 1**). The complex was obtained by coordination of ligand with Cu^{2+} metal ion in a 1 : 1 molar ratio. Both HL and its corresponding Cu-chelate were characterized by various spectral techniques including ^{1}H-NMR, ^{13}C-NMR, infrared, electronic and mass spectra, CHN analysis and magnetic susceptibilities. CuL was found to be highly stable in the air as a solid and in liquid phases. The thermal stability of CuL was tested at a high temperature (211 °C). No decomposition was observed, which showed very high thermal stability. Both ligand (HL) and complex (CuL) were highly soluble in polar organic solvents e.g. methanol, ethanol and acetonitrile. Low solubility was observed in less polar solvents ($CHCl_3$, CH_2Cl_2 and benzene), whereas, DMF and DMSO showed fair solubility. Various attempts were made to crystallize the complex to get a single-crystal for X-ray analyses but no luck so far. The C, H, N-elemental analysis data for HL and its Cu-chelate are documented in **Table 1**. The measured values are agreed with the calculated values of their tentative structures, with the slight acceptable differences (about ± 0.4 %) referring to the high purity of ligand (HL) and complex (CuL). The magnetic features of CuL showed that CuL is paramagnetic with a magnitude 2.77 B.M. confirming that copper ion is divalent with d^9 electronic configuration. ^{1}H NMR and ^{13}C NMR spectra of HL are presented in **Figs. S1 and S2**.

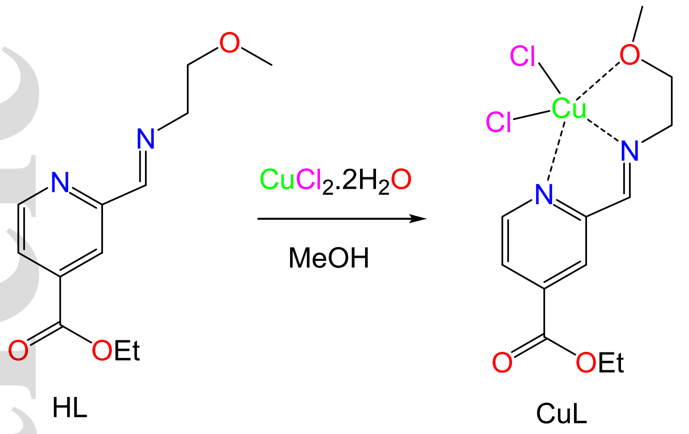

Scheme 1. Synthesis of Cu(II)-complex (CuL) from (*E*)-ethyl-2-((2-methoxyethylimino)methyl)isonicotinate (HL)

In ^{1}H-NMR spectra (**Fig. S1**), the HL showed a characteristic peak for —CH=N— proton which appeared at 8.72 ppm as a doubled. The other three signals in the aromatic region belong to the pyridine ring appeared at 8.46, 8.42 and 7.83 ppm. Two protons signals appeared at 4.38 and 3.85 ppm with two proton integration each, belong to the neighbors —CH_2— of —CH=N— group. A signal at 3.33 ppm with the integration of three protons belongs to the methoxy group. The ethyl ester protons showed signals at 3.71 and 1.38 ppm for the —CH_2— and —CH_3 protons, respectively. The most distinguished signal in ^{13}C NMR spectra is at 164.80 ppm, which assigned to —CH=N— group (**Fig. S2**, in the supplementary materials).

FT-IR absorption frequencies of the ligand (HL) were measured for comparison with complex upon coordination. The ligand Schiff base group (—CH=N—), which showed the IR spectral band at 1682 cm^{-1} was strongly shifted to 1611 cm^{-1} in the complex (CuL) due to nitrogen lone pair coordination to Cu^{2+} ion. The second distinguished vibrational band of the —CH=N— group of the pyridine ring was also shifted from 1625 to 1559 cm^{-1} upon coordination of pyridine nitrogen to the central metal ion.[69] Moreover, the C—O vibrational band of the coordinated methoxy group was also strongly shifted from 1344 cm^{-1} to low frequencies region 1282 cm^{-1}, as shown in **Scheme 2**. Importantly, there were a number of new weak bands observed at 687 and 439 cm^{-1}, which considered for the vibrational spectra of the coordination bonds Cu—O and Cu—N, respectively.[70]

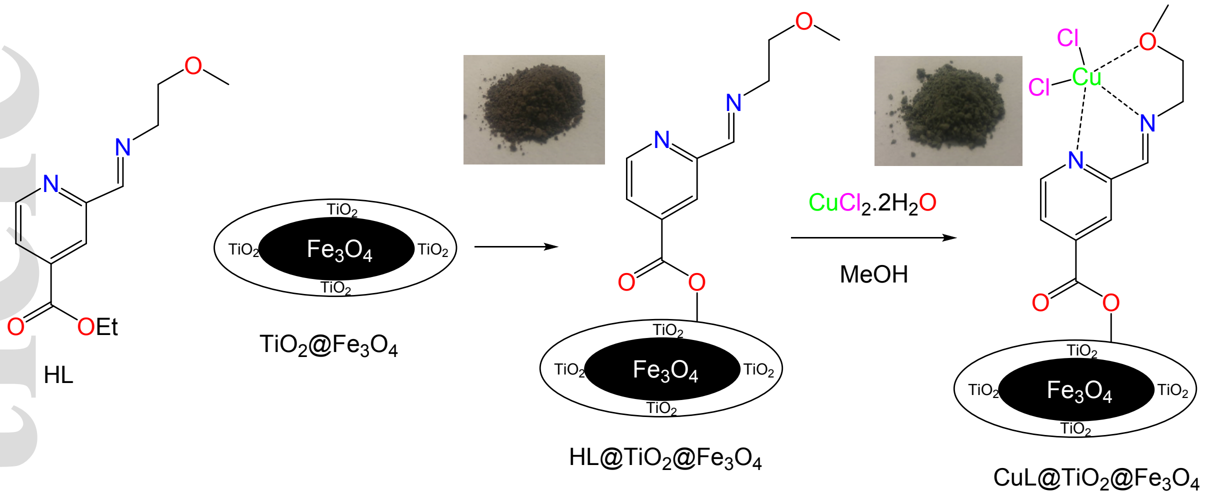

Scheme 2. The absorbed progressed steps of Cu-complex (CuL) on the $Fe_3O_4@TiO_2$.

The electronic transitions of HL and CuL were investigated in methanolic solution at room temperature with the assignment of their maximum absorption wavelength (λ_{max}) and molar absorptivity, which summarized in **Table 1** and presented in **Fig. 1**. In the UV-region, HL displayed one specific high-energy band for $\pi \rightarrow \pi^*$ and/or $n \rightarrow \pi^*$ transitions in the molecule at 321 nm. Furthermore, an additional electronic absorption band at 334 nm, which interpreted the electronic ligand charge transition.[71] Considerably, the coordination bonding between HL and Cu^{2+} ion caused newly observable shifts of the $\pi \rightarrow \pi^*$ and/or $n \rightarrow \pi^*$ characteristic bands of the ligand. Particularly, that transition was shifted to lower energy magnitudes at 301 nm for CuL. Indeed, the ligand charge transfer band was disappeared after complexation with Cu^{2+} ion with the presence of a novelty band in the visible region due to the d→d transition, which appeared at 647 nm (**Fig. 1**).

The mass spectra of HL and CuL were measured in methanolic media. The mass spectroscopic results are shown in **Fig. S3 and S4**. Mass spectra of HL presented distinguished peaks at 236.9, 258.9, 265.9 and 291.1 (high intense) m/z confirming the molecular structure of the ligand. CuL established two mass peaks one at 368.6 and the other was 369.9 m/z for the molecular mass of the complex and a high intense base peak at 299.2 m/z for the complex molecular mass without the two chloride ions $[M - 2\ Cl^-]$.

3.2 | Structural formation and characterization of Fe_3O_4, $TiO_2@Fe_3O_4$ and $CuL@TiO_2@Fe_3O_4$ nanoparticles

CuL was immobilized on Fe_3O_4-NPs coated by TiO_2 within the ethoxy group, as reported previously.[32] Sadeghzadeh et *al.* reported that manganese (II) complex of imine complex has been supported on Fe_3O_4-NPs within the ethoxy moiety as an effective heterogeneous catalyst for benzopyranopyrimidines syntheses.[72] Also, Eftekhari-Sis et *al.* synthesized immobilized Oxoperoxo tungsten (VI) Schiff base complex within the ethoxy moiety, as a catalyst for alcohol oxidation.[73] The significant FT-IR spectral bands for CuL and its support on $TiO_2@Fe_3O_4$ are assigned in **Fig. 2**. A significant vibrational band at 550 cm^{-1} was remarked for the free Fe_3O_4 pure magnetic nanoparticles for the Fe—O bond.[74] Water molecules exhibited characteristic bands at 3177 and 1617 cm^{-1} for the O—H group in Fe_3O_4 (**Fig. 2a**) and also at 3196 and 1635 cm^{-1} for $TiO_2@Fe_3O_4$ (**Fig. 2b**).[70,75] The stretching band of the Fe—O bond was lower shifted due to the coating of TiO_2 to appear at 485 cm^{-1}. Particularly, other distinguished bands at 2117 and 1345 cm^{-1} for Fe_3O_4 and at 2919 to 2850 cm^{-1} for $TiO_2@Fe_3O_4$ were characterized for the N≡C—O bonding of urea which used as a chelating agent in preparing process of Fe_3O_4.[76] The presence of new vibrational bands at 718 and 555 cm^{-1} were characteristic for the Ti—O—Ti bonding mode.[77] The specific stretching bands of un-supported free CuL, which displayed at 1724 and 1282 cm^{-1} for the C=O and C—O bonds, respectively, were little influenced by the immobilization on $TiO_2@Fe_3O_4$ nanoparticles to appear at 1735 and 1291 cm^{-1} (**Figs. 2c,d**). A high remarkable disappearance of the aliphatic C—H band at 2925 and the C—O band at 1211 cm^{-1} could be proven for the Cu-complex immobilization on $TiO_2@Fe_3O_4$ with lose of ethyl group of the *para*-ethyl ester group, as detected previously.[77] Indeed, the intensity of the absorption bands of —CH=N— Schiff base, —CH=N— pyridine and CH—N groups at 1611, 1559 and 1111 cm^{-1}, respectively, were reduced from moderate and strong bands in the free CuL to be weak bands after its supporting on $TiO_2@Fe_3O_4$ (**Fig. 2d**).[78] Moreover, the Ti—O—Ti bonding mode assigned vibrational stretching bands at 725 and 523 cm^{-1}, which also small influenced by the insertion of high magnetic particles of Fe_3O_4 and CuL, as shown in **Scheme 2**.

The energy-dispersive X-ray spectroscopy analysis (EDS) was applied to investigate the chemical composition of the prepared material in addition to the degree of its purity. **Fig. 3** presents the obtained EDS spectra of prepared Fe_3O_4, $TiO_2@Fe_3O_4$ and $CuL@TiO_2@Fe_3O_4$ samples. **Figure 3a** reveals high contents of Fe and O ions which reflect the high purity of the prepared Fe_3O_4 sample. **Figure 3b** exhibits high peaks attributed to the presence of Ti in the shell of the Fe_3O_4 nanoparticles core. However, there are some small signal peaks of Fe ions were detected as a consequence of an irregular coating of $TiO_2@Fe_3O_4$. Likewise, it was seen that there are clear peaks located at well-defined positions attributed to Fe, O, Ti, C, N and Cu atoms as shown in **Fig. 3c**. This could be a shred of evidence for the presence of all mentioned elements in the structural formation of the CuL@TiO_2@Fe_3O_4 prepared sample.

The surface morphology of Fe_3O_4, TiO_2@Fe_3O_4 and CuL@TiO_2@Fe_3O_4 samples were analyzed using FE-SEM and HR-TEM techniques. The FE-SEM images represented in **Figs. 3a-c** show the surface morphology of the target samples. **Figure 3a** exhibited Fe_3O_4 composed of a uniform nanoparticles-like spherical structure. While the image of **Fig. 3b** revealed the surface morphology of Fe_3O_4 nanospheres after coated by TiO_2. This coated layer of TiO_2 causes the accumulation of nanospheres of Fe_3O_4 forming the bigger ones, which lead to an increase in the degree of the crystalline nature of the TiO_2@Fe_3O_4 samples. **Figure 3c** displayed the surface of the morphology of Fe_3O_4 after coated by both of TiO_2 and CuL complex to form heterostructure of CuL@TiO_2@Fe_3O_4. It could be observed that the structure of the sample is composed of both agglomerated nanospheres and deformed nanorods. Irregular agglomeration of TiO_2@Fe_3O_4 nanoparticles was cross-linked with deformed nanorods shaped structures of CuL organic framework. This imperfection of structure compared to the structure of Fe_3O_4 nanoparticle was considerably due to the changes in the atomic coordination, dangling bonds and lattice disorder, which resulted from coated layers of TiO_2 and CuL.[79]

Figs. 4 represent the HR-TEM micrographs of Fe_3O_4, TiO_2@Fe_3O_4 and CuL@TiO_2@Fe_3O_4 samples. These images supported the result obtained from FE-SEM images. A seen in **Fig. 4a**, a uniform nanospheres shaped structure of Fe_3O_4 was formed, whereas **Fig. 4b** shows nanoclusters of Fe_3O_4 nanoparticles coated by TiO_2 form core-shell of TiO_2@Fe_3O_4. The amorphous shell of TiO_2 covered Fe_3O_4 nanoparticles reduced the degree of crystallization of Fe_3O_4 and enhanced disorders, defects and porosity of its surface morphology, which has improved the degree of adsorption capacity. **Figure 4c** revealed Fe_3O_4 coated by two layers of TiO_2 and CuL complex. The structure morphology of the heterostructure CuL@TiO_2@Fe_3O_4 formed an irregular shape of texture composed of aggregates of clusters of TiO_2@Fe_3O_4 cross-linked with deformed nanorods of CuL complex.

An X-ray diffraction (XRD) analysis of Fe_3O_4 nanoparticles, TiO_2@Fe_3O_4 and CuL@TiO_2@Fe_3O_4 samples are depicted in **Figs. 5**. As shown in **Fig. 5a**, the multiple diffraction peaks indicated the observed planes of Fe_3O_4.[80] With the aid the standard JCPDS database of Fe_3O_4 (JCPDS, card No. 75-1609),[81] the peaks locate at 2θ of 20.5°, 35.4°, 37.2° and 57.1° preferred orientations planes at (1 1 1), (3 1 1) and (5 1 1), respectively.

Figure 5b exhibits the XRD pattern of Fe_3O_4 after coated by TiO_2 ($TiO_2@Fe_3O_4$), which existed in anatase crystallographic phase and presented many peaks referring to the different planes. The peaks at 2θ of 20.5^{o}, and 37.2^{o}, with preferred orientations planes at (1 1 1) and (3 1 1), respectively, were related to Fe_3O_4 cores, which confirmed its magnetite phase. Whereas, the peaks at 2θ of 24.3^{o}, $26.9.2^{o}$ and 36.9^{o} with preferred orientations planes at (1 0 1), (1 1 0) and (0 0 4), respectively, were attributed to the TiO_2 shell.[81] **Figure 5c** shows the XRD pattern of Fe_3O_4 after coated by a double layer of TiO_2 and Cu(II)-complex ($CuL@TiO_2@Fe_3O_4$). The XRD spectrum of the sample revealed more multiple new peaks related to the CuL coated shell. This could assign that Fe_3O_4 cores are coated completely with externally two shells of TiO_2 and CuL. The present result of XRD analysis exhibited well agreement with that of FE-SEM and HR-TEM micrographs.

Figure 6 presents the applied magnetic field dependence of the magnetization characteristics (M–H curves) at 25 °C for Fe_3O_4 purely nanoparticles, $TiO_2@Fe_3O_4$ and $CuL@TiO_2@Fe_3O_4$ samples. It could be seen that there was no hysteresis loops are detected. Hence, the remnants magnetization and coercivity were absent for those samples leading to the superparamagnetic behavior. The saturation magnetization of Fe_3O_4 nanoparticles was about 60 emu/g, which could be much greater than those of the $TiO_2@Fe_3O_4$ (40 emu/g) and $CuL@TiO_2@Fe_3O_4$ (22 emu/g). The stable ferrite phase in the presence of the Fe_3O_4 layer revealed the superparamagnetic properties of Fe_3O_4-NPs. However, the reduction in magnetization values of $Fe_3O_4@TiO_2$ was most likely attributed to the nonmagnetic shell of TiO_2 coated cores of the magnetic Fe_3O_4 nanoparticles. Further reduction in the magnetization of $CuL@TiO_2@Fe_3O_4$ was remarked since the presence of an additional shell of nonmagnetic species of CuL complex coated $TiO_2@Fe_3O_4$ sample rapidly decreased its magnetic properties compared to Fe_3O_4 and $TiO_2@Fe_3O_4$ samples.[82]

TGA of CuL and $CuL@TiO_2@Fe_3O_4$ depicts two different degradation steps, as shown in **Fig. 7**. CuL presented distinguished three degrading steps, whereas, $CuL@TiO_2@Fe_3O_4$ did not show any characteristic decomposition steps. The loss within 180–200 °C was probably due to the loss of moisture and CO_2 in the Cu-complex with 9.1%.[2,3] The second weight loss was found in the region from 250–300 °C gradually presumed to the degradation of the organic moiety in CuL with 31.2%.[83] The weight loss in the third stage was observed at the range 300 to 320 with gradual degradation and with a loss percentage of 39.9%. Comparatively, the supported CuL on the surface of $TiO_2@Fe_3O_4$ showed high thermal stability compared to the free CuL. This result could propose that CuL@TiO_2@Fe_3O_4 is highly stable and could be utilized as a heterogeneous catalyst up to 340 °C without any observable degradation.

The Brunauer-Emmett-Teller (BET) method is a widely applicable tool to characterize the pore structure and the physical and chemical adsorption of gas molecules on the specific surface area of materials. **Figure 8** reveals the characteristic adsorption-desorption isotherms of CuL@TiO_2@Fe_3O_4 core-shells, which taken for N_2 at 77.4 K. Based on BET classifications, the isotherm curve of the core-shells sample exhibited a type IV profile with an H3-type hysteresis loop, which reflected the mesoporous nature for CuL@TiO_2@Fe_3O_4 sample. The adsorption-desorption isotherm curve revealed an evident hysteresis loop at the relative pressure (P/P_o) > 0.34, which was a characteristic porous material. Whereas, the adsorption and desorption curves almost coincided under the low value of $P/P_o \leq 0.34$. This process was associated with capillary condensation in mesopores. According to the IUPAC classifications, the pores within porous materials could be classified into micropores (< 2nm), mesopores (2 – 50 nm) and macropores (> 50 nm). The average pore radius for CuL@TiO_2@Fe_3O_4 sample was found to be 2.12 nm, which reflected the mesopores nature. Additionally, the total pore volume was also estimated to be 0.043 cc/g. Therefore, it well-known that the Fe_3O_4 powder had negligible N_2-adsorption and it was called a non-porous material.[84] The porosity of CuL@TiO_2@Fe_3O_4 core-shells enhanced and thus leading to the significantly improved its adsorption capacity.

Furthermore, the BET specific surface of the sample can be estimated *via* the well-known BET equation as the following **Eq. 1**[85,86]:

$$\frac{1}{v\left(\frac{P}{P_o}\right)-1}=\frac{c-1}{v_m c}\left(\frac{P}{P_o}\right)+\frac{1}{v_m c} \qquad (1)$$

where, P and P_o are equilibrium and saturation pressure of adsorbents, respectively, v is the adsorbed gas quantity and v_m is the monolayer adsorbed gas quantity and c is the BET constant. **Eq. 1** could be applicable at $P/P_o = 0.05 - 0.3$ for the surface area of macro- and mesoporous materials.

Figure 9 revealed the BET surface area plot of CuL@TiO_2@Fe_3O_4. The best fit result exhibited straight line and according to **Eq. 1**, the value of v_m and c could be extracted from the value of the slope ~ 17.96 and the y-intercept of that line ~ 0.805 in **Fig. 9**. The value of the BET constant (c)

was found to be 23.3. Moreover, the BET specific surface area (S_{BET}) could be given in terms of the total surface area S_{Total}, as shown in **Eqs. 2 and 3**:

$$S_{BET} = \frac{S_{Total}}{a} \qquad (2)$$

and

$$S_{Total} = \frac{v_m N s}{V} \qquad (3)$$

where, *s* is the adsorption cross-section of the adsorbing species ~ 16 Å^2/molec, *N* is Avogadro's number, *V* is the molar volume of the adsorbate gas and *a* is the mass of the solid sample ~ 0.0216 g. The value of S_{BET} was estimated to be ~ 185.54 m^2/g.

The present value of S_{BET} was comparable with those obtained by other works in literatures[87,88] for analogy core-shell systems. It could be observed that the value of S_{BET} of CuL@TiO_2@Fe_3O_4 core-shell-shell system was the largest value. Zhang et *al.*[87] reported the value of S_{BET} of Fe_3O_4-C-TiO_2 was found to be ~ 40 m^2/g. Likewise, Lee et *al.*[88] prepared a Fe_3O_4-SiO_2 sample with S_{BET} of ~ 41 m^2/g. Whereas, Costa et *al.*[89] synthesized Fe_3O_4-SiO_2-TiO_2 with S_{BET} of ~ 141 m^2/g. Here, the largest S_{BET} was the benefit of adsorption, influenced by its large surface area with large adsorption. This result indicated that the surface area of Fe_3O_4-nanoparticles was increased by coating with TiO_2 and CuL. Hence, the CuL@TiO_2@Fe_3O_4 core-shell-shell system obtained in the present work could be considered as a potential candidate to be used as a heterogeneous catalyst.

3.3 | Catalytic cross-coupling reactions

Exploring the catalytic potential of the novel prepared catalysts, CuL and CuL@TiO_2@Fe_3O_4 were devoted to the C—C cross-coupling reaction (Suzuki-Miyaura) of phenylboronic acid with 2-pyridyl bromide and chloride, and to the C—N cross-coupling reaction (Buchwald-Hartewig) of 2-aminopyridine with 2-pyridyl bromide and chloride. Utilized optimized reaction conditions using K_2CO_3 as a base and ethanol as a solvent at 100 °C for the given time. The kinetics of the homogeneously and heterogeneously catalyzed reaction using CuL and CuL@TiO_2@Fe_3O_4 catalysts, respectively, were determined by the yield percentages of the chemoselective C—C and C—N biaryl synthesis, as listed in **Table S2**. Reaction progress was monitored by TLC (thin column chromatography) and the yield percentages of the C—C and C—N biaryl products were determined by GC-MS. The results, which plotted in **Figs. 10a,b**, showed that both catalysts consumed coupling reagents in different times frames. CuL took 4 h to afford the highest yield of the C—C coupling product provided 89% yield while the CuL@TiO_2@Fe_3O_4 catalyst took 6 h with the highest yield 91%of the reaction completion. Similarly, for C—N coupling, CuL took 3 h with 91% yield and CuL@TiO_2@Fe_3O_4 took one hour longer (4 h) with 94% yield to complete the cycle. The slight variation in consumption time for both catalysts, 2 h difference for C—C coupling and 1 h for C—N coupling could be the less homogenicity of CuL@TiO_2@Fe_3O_4 in the reaction media.[39] The slightly higher percentage yield of the desired products (C—C and C—N biaryls) with CuL@TiO_2@Fe_3O_4 catalyst than that with CuL catalyst could be interpreted by the presence of the supporting materials of TiO_2 and Fe_2O_3, which enhanced the catalytic reactivity of the immobilized CuL catalyst within increase in the surface area of TiO_2@Fe_2O_3, as detected above.[19,20] During optimization, various reaction conditions were examined including different solvents, e.g. ethanol, chloroform, toluene, water and ethanol-aqueous equimolar mixture, various bases (K_2CO_3, *t*BuOK and K_3PO_4) and reaction time at 100 °C.

The yield percentages for both C—C and C—N cross-couplings are represented in **Tables 2 and 3**, respectively. The results from **Tables 2 and 3**, it could be noted that the C—N coupling product yield percentages were better than those of C—C coupling products, which could be estimated from the low stability of boronic acid derivatives in an aerobic atmosphere compared to that of amino group of 2-aminopyridine, as a precursor.[1] In a blank reaction, *i.e.* in absence of any catalyst, Suzuki-Miyaura reaction was tested obtaining low yield product percentages, *i.e.* 16 and 28% (**Table 2**, entries 1 and 2), respectively.

It is well documented that the inorganic bases give usually the best results of yield percentages for the C—C[90] and C—N chemoselectivities.[2] K_2CO_3 was found to be the best base for such catalytic systems, in contrast to other used bases, *i.e.* *t*BuOK, K_3PO_4 and KOH. The reason could be that K_2CO_3 is more compatible with the catalyst and solvent than the other tested bases, as observed previously.[91] With various solvents K_2CO_3 showed better performance (**Tables 2 and 3**) than other used bases. KOH was found to be the least active base in both catalytic reactions provided low yield for C—C biaryls synthesis (entires 7 and 8 in **Table 2**, 37 and 44% catalyzed by CuL and CuL@TiO_2@Fe_3O_4, respectively). Similarly, for the C—N cross-coupling, the yield was also low with KOH, as observed in **Table 3** (entries 5 and 6, giving 42 and 49 % catalyzed by CuL and

CuL@TiO_2@Fe_3O_4, respectively). The high basicity of the reaction media could cause base hydrolysis,[92] with formation probably of $Cu(OH)_2$ precipitate.[93,94]

The other applied base, *i.e.* *t*BuOK presented appreciable potential towards the formation of the C—C biaryls from the aryl bromide in various solvents *e.g.* toluene, water, ethanol and ethanol-water binary mixture (**Table 2**, entries 7, 21, 29, and 37 catalyzed by CuL offered 65, 62, 76 and 70%, and also entries 9, 23, 31 and 39 catalyzed by CuL@TiO_2@Fe_3O_4 awarding 72, 59, 80 and 72% of the chemoselective product, respectively). Likewise, the catalytic system with K_3PO_4 displayed good potential with good yield percentages of the C—C biaryls in various solvents, in toluene (entry 8, 53%), water (entry 22, 55%), ethanol (entry 30, 81%) and ethanol-water binary mixture (entry 37, 70%) with homogeneous catalyzed system (CuL). In heterogeneous reaction condition (CuL@TiO_2@Fe_3O_4), the yield percentages were clearly influenced by the solvent, in toluene (entry 10, 66%), water (entry 24, 51%), ethanol (entry 32, 79%) and ethanol-water binary mixture (entry 40, 70%).

By using K_3PO_4 in C—N cross-coupling system, the obtained yields were moderate to good with CuL (**Table 3**), as 69% in toluene (entry 6), 55% in water (entry 20), 75% in ethanol (entry 28) and 70% in EtOH-H_2O mixture (entry 36). K_3PO_4, also reflected good behavior towards the catalytic potential of CuL@TiO_2@Fe_3O_4, as 75% in toluene (entry 8), 59% in water (entry 22), 72% in ethanol (entry 30) and 74% in EtOH-H_2O mixture (entry 38). It could be concluded that K_3PO_4 is a relatively good base, as reported recently.[95]

The reactivity of the homogeneous (CuL) and heterogeneous (CuL@TiO_2@Fe_3O_4) catalyst in various tested solvents in C—C and C—N bond formation was found to be in order ethanol > chloroform > toluene > ethanol-water mixture > water. For both homogeneous and heterogeneous phases, ethanol was found to be the best choice, the reason could the better solubility of the reaction contents and their miscibility could improve their catalytic sufficiency towards C—C and C—N cross-couplings.[17] Interestingly, after ethanol, chloroform also showed good compatibility with these catalytic systems (**Tables 2 and 3)**. In ethanol-water mixture and in water alone, the probed reactions demonstrated lower yield percentages of the target products (**Table 2**, entries 17-23 for water and entries 33-40 for ethanol-water equimolar mixture) (**Table 3**, entries 15-22 for water and entries 31-38 for ethanol-water equimolar mixture). Water as a high polar inorganic solvent did not show the desired performance, the reason could be the poor solubility of the organic contents in the reaction media.[79,96] For that reason, the catalytic potential of CuL and CuL@TiO_2@Fe_3O_4 were remarkably reduced and offered the lowest yield (**Tables 2 and 3**).

As a more reactive coupling partner 2-pyridyl bromide offered better coupling results then 2-pyridyl chloride, as summarized in **Tables 2 and 3**. The high bond dissociation energy of the Ar—Cl bond could be the reason for the lower reactivity of 2-pyridyl chloride.[97]

To demonstrate the role of feeding of CuL complex to $TiO_2@Fe_3O_4$, separated probes of catalytic tests of C—C cross-coupling reactions of phenylboronic acid with 2-pyridyl bromide at the optimized reaction conditions (in presence K_2CO_3, in ethanol at 100 °C for 6 h) using Fe_3O_4 and $TiO_2@Fe_3O_4$ were accomplished and their results of the product yields are represented in **Table 4**. The yield percentages of the C—C biaryl product catalyzed by Fe_3O_4 (only) awarded 71% and within $TiO_2@Fe_3O_4$ (as a heterogeneous catalyst) gave 83% (**Table 4**). Comparatively, the immobilized CuL to the $TiO_2@Fe_3O_4$ nanoparticles promoted its surface area and hence improved its catalytic sufficiency (affording 91% of the desired product).

Using the best base (K_2CO_3) solvent (ethanol) combination, the reaction was further investigated for catalytic loading using 0.01, 0.02, 0.05 and 0.1 mmol of CuL and 0.05, 0.1 0.2 and 0.5 g of $CuL@TiO_2@Fe_3O_4$ in C—C cross-coupling of phenylboronic acid with 2-pyridyl bromide. The results are summarized in **Table 5**. For CuL, the increased loaded amounts of the catalyst from 0.01, 0.02 to 0.05 mmol, showed observable performance in the yield percentages from 78, 89 to 89%, similarly, the increased loaded amounts of $CuL@TiO_2@Fe_3O_4$ catalyst (0.1 mmol of CuL and 0.5 g) also showed prominent improvement in the yield percentages (73, 90 and 91 of C—C product), **Table 5**. The highest loaded amounts of both catalysts (0.1 mmol of CuL and 0.5 g of $CuL@TiO_2@Fe_3O_4$) indicated rejection by the catalytic system, which awarded lower yield compared to the lower loaded amounts (81 and 89%, respectively). The high loaded amount of both catalysts could observably catalyze the reaction for further by-products.[98,99]

Tables 6 and 7 display the yield products of Suzuki-Miyaura and Buchwald-Hartwig cross-couplings of phenylboronic acid or 2-aminopyridine with alternative heterocyclic bromides, as coupling partners, under optimized conditions catalyzed by either CuL or $CuL@TiO_2@Fe_3O_4$.

Interestingly, the biaryls and secondary diaryl amines were obtained within single regioisomers, which afforded good yields. With 2-bromothiophene and 2-bromofuran, the catalysts worked with lower activity and the yields were good (60 and 67% for CuL and $CuL@TiO_2@Fe_3O_4$, respectively) for the Suzuki-Miyaura reaction (**Table 6**). Whereas, in respect of the Buchwald-Hartwig reactions, the reactivity of CuL and$CuL@TiO_2@Fe_3O_4$ was somewhat lower and gave lower yield (53 and 64% for 2-bromothiophene and 2-bromofuran, as small heterocyclic reagents, respectively, **Table 7**). As a consequence, overall, the more electron-withdrawing aryl bromides gave a better yield of C—C and C—N products more than those of the less electron-withdrawing aryl bromides with both catalysts, as for particularly for 2-pyridyl bromide, 3-pyridyl bromide, 4-pyridyl bromide, 2-quinolyl bromide and 8-quinolyl bromide.

For understanding the tolerance of the electronic effects of the heterocyclic attached ring to bromide Ar—Br, the heterocyclic bromides with more electron-withdrawing more resonance character would increase the nucleophilic power of bromide and hence, reinforce it reactivity towards cross-couplings.[100]

Comparatively, the catalytic yield results of the C—N cross-coupling reaction catalyzed by new magnetic Cu(0)-amino acid catalyst immobilized on Fe_3O_4-TiO_2-L-dopa afforded 80% of the biaryls between aniline and phenylboronic acid in water and in presence of K_2CO_3 at 80 °C for 24 h.[2]

3.4 | Reusability of the homogeneous and heterogeneous CuL

The recyclability of the Cu-catalysts homogeneously (with CuL) and heterogeneously (with CuL@TiO_2@Fe_3O_4) were examined in C—C cross-coupling reaction, using phenylboronic acid with 2-pyridyl bromide in the presence of K_2CO_3, at the optimum conditions in toluene. The obtained results are displayed in **Fig. 11**. The homogeneous catalyst (CuL) was separated easily from the reaction mixture by extracting and filtration after cooling down to the room temperature and washed by toluene. While, the heterogeneous catalyst (CuL@TiO_2@Fe_3O_4) was extracted easily by a magnet from the reaction mixture, washed with toluene, dried in an oven and reused in the next trial using fresh solvent and reagents. The reusability of homogeneous catalyst (CuL) was found to be limited up to 3 times only, whereas the heterogeneous catalyst (CuL@TiO_2@Fe_3O_4) showed better catalytic performance in cycling up to 7 times. In the homogeneous phase catalysis, the catalyst lost its potential dramatically on the fourth consecutive run. It lost more than half of its reactivity that could be explained by its decomposition or loss of little quantity in the extraction process.

After 8 times, in the heterogeneous CuL@TiO_2@Fe_3O_4 showed remarkable inhibition of its reactivity is almost ~10% without loss of its composition. **Figure 12** presents the EDS analyses of the reused CuL@TiO_2@Fe_3O_4 after 7 times, as observed elsewhere.[101] Clearly, there was no considered change in the morphology of CuL@TiO_2@Fe_3O_4 to lose its catalytic potential, so, there is no obvious reason for its deactivation, which could be found elsewhere or could explain that behavior.

4 | CONCLUSIONS

N,*N*,*O*-tridentate pyridyl-imine ligand (HL) was synthesized and then treated with $CuCl_2$ to give a novel mononuclear copper complex (CuL). Both ligand (HL) and its complex (CuL) were characterized by various spectral tools, *i.e.* NMR, IR, UV-Vis. and EI spectra, and elemental analyses. For heterogeneous catalysis, the novel complex was synthesized afresh by immobilizing the ligand on TiO_2 coated Fe_2O_3 nanoparticles, provided solid-supported copper catalyst (HL@TiO_2@Fe_3O_4). The different analytical techniques (FT-IR, XRD, SEM, TEM, EDS, TGA and magnetism) were used to confirm the elemental compositions and morphological structure of CuL@TiO_2@Fe_3O_4 core-shell-shell system. The surface morphology of Fe_3O_4, TiO_2@Fe_3O_4 and CuL@TiO_2@Fe_3O_4 were analyzed by using FE-SEM and HR-TEM techniques, which exhibited agglomerations of TiO_2@Fe_3O_4 nanoparticles, which are cross-linked with deformed nanorods shaped structure of CuL organic framework. The BET isotherm curve of the CuL@TiO_2@Fe_3O_4 exhibited a type IV profile with an H3-type hysteresis loop, which reflected the mesoporous nature with an average pore radius ~ 2.12 nm and BET specific surface S_{BET} ~ 185.54 m^2/g. Both catalysts were investigated in catalysis for Suzuki-Miyaura (C—C bond formation) and Buchwald-Hartwig amination (C—N bond formation) reactions. Both catalysts CuL and CuL@TiO_2@Fe_3O_4 showed prominent catalytic potential under the optimized reaction conditions. The solid supported catalyst (CuL@TiO_2@Fe_3O_4) showed a slightly dominant catalytic reactivity over a homogeneous catalyst system (CuL). Hence, the characteristic obtains interpreted the catalytic potential of the current samples, in which the increase of the surface area of TiO_2@Fe_3O_4 with immobilized CuL, progressed its catalytic reactivity. In C—C cross-coupling reaction the heterogeneous catalyst (CuL@TiO_2@Fe_3O_4) was recycled up to 7 times, while homogeneous catalyst (CuL) up to 3 times only.

ACKNOWLEDGMENTS

The authors acknowledge the Deanship of Scientific Research at King Faisal University for the financial support under Nasher Track (Grant No. 186374).

REFERENCES

[1] Lennox AJJ, Lloyd-Jones GC/Selection of boron reagents for Suzuki–Miyaura coupling. Chem. Soc. Rev. 2014;42:412-443.

[2] Sharma H, Mahajan H, Jamwal B, Paul S/Cu@Fe_3O_4-TiO_2-L-dopa: A novel and magnetic catalyst for the Chan-Lam cross-coupling reaction in ligand free conditions. Catal. Commun. 2018;107:68-73.

[3] Anuma S, Mishra P, Bhat BR/Copper complex with N-,O-architecture grafted graphene oxide nanosheet as a heterogeneous catalyst for Suzuki cross coupling reaction. J. Taiwan Inst. Chem. Eng. 2019;95:643-651.

[4] Dutta DK, Borah BJ, Sarmah PP/Recent Advances in Metal Nanoparticles Stabilization into Nanopores of Montmorillonite and Their Catalytic Applications for Fine Chemicals Synthesis. Catal. Rev. 2015;57:257-305.

[5] Du J, Qi J, Wang D, Tang ZY/Facile synthesis of Au@TiO_2 core–shell hollow spheres for dye-sensitized solar cells with remarkably improved efficiency. Energy Environ. Sci. 2012;5:6914-6918.

[6] Huang K, Zhang L, Xu T, Wei H, Zhang R, Zhang X, Ge B, Lei M, Ma J-Y, Liu L-M, Wu H/−60 °C solution synthesis of atomically dispersed cobalt electrocatalyst with superior performance. Nat. Commun. 2019;10:606-616.

[7] Yang H, Geng L, Zhang Y, Chang G, Zhang Z, Liu X, Lei M, He Y/Graphene-templated synthesis of palladium nanoplates as novel electrocatalyst for direct methanol fuel cell. Appl. Suf. Sci. 2018;466:385-392.

[8] Huang K, Wang R, Wu H, Wang H, He X, Wei H, Wang S, Zhang R, Lei M, Guo W, Ge B, Wu H/Direct immobilization of an atomically dispersed Pt catalyst by suppressing heterogeneous nucleation at −40 °C. J. Mater. Chem. A 2019;7:25779-25784.

[9] Nasrollahzadeh M, Issaabadi Z, Khonakdar HA, Wagenknecht U/Synthesis, characterization and catalytic activity of Fe_3O_4@SiO_2 nanoparticles supported copper(II) complex as a magnetically recoverable catalyst for the reduction of nitro compounds, Nigrosin and Methylene blue. Sep. Purif. Technol. 2018;203:185-192.

[10] Keyhaniyan M, Shiri A, Eshghi H, KhojastehnezhadA/Novel design of recyclable copper(II) complex supported on magnetic nanoparticles as active catalyst for Beckmann rearrangement in poly(ethylene glycol). Appl. Organometal. Chem. 2018;32:e4344.

[11] Sarkheil M, Lashanizadegan M/Copper(II) Schiff Base Complex Immobilized on Superparamagnetic Fe_3O_4@SiO_2 as a Magnetically Separable Nanocatalyst for Oxidation of Alkenes and Alcohols. Appl. Organometal. Chem. 2017;31:e3726.

[12] Esmaeilpour M, Javidi J, Dodeji FN, Abarghoui MM/M(II) Schiff base complexes (M = zinc, manganese, cadmium, cobalt, copper, nickel, iron, and palladium) supported on superparamagnetic Fe_3O_4@SiO_2 nanoparticles: synthesis, characterization and catalytic activity for Sonogashira–Hagihara coupling reactions. Transition Met. Chem. 2014;39:797-809.

[13] Moradi-Shoeili Z/Immobilized Cu(II)–Schiff base complex on modified Fe_3O_4 nanoparticles as catalysts in the oxidation of *o*-phenylenediamine to 2,3-diaminophenazine. Reac. Kinet. Mech. Cat. 2017;120:323-332.

[14] Elhamifar D, Mofatehnia P, Faal M/Magnetic nanoparticles supported Schiff-base/copper complex: An efficient nanocatalyst for preparation of biologically active 3,4-dihydropyrimidinones. J. Colloid Interface Sci. 2017;504:268-275.

[15] Esmaeilpour M, Sardarian AR, Javidi J/Schiff base complex of metal ions supported on superparamagnetic Fe_3O_4@SiO_2 nanoparticles: An efficient, selective and recyclable catalyst for synthesis of 1,1-diacetates from aldehydes under solvent-free conditions. Appl. Catal. A 2012;445-446:359-367.

[16] Esmaeilpour M, Sardarian AR, Javidi J/Synthesis and characterization of Schiff base complex of Pd(II) supported on superparamagnetic Fe_3O_4@SiO_2 nanoparticles and its application as an efficient copper- and phosphine ligand-free recyclable catalyst for Sonogashira–Hagihara coupling reactions. J. Organomet. Chem. 2014;749:233-240.

[17] Miyaura N, Suzuki A/Palladium-catalyzed cross-coupling reactions of organoboron compounds. Chem. Rev. 1995;95:2457-2483.

[18] Bahrami K, Khodaei MM, Meibodi FS/ Suzuki and Heck cross-coupling reactions using ferromagnetic nanoparticle-supported palladium complex as an efficient and recyclable heterogeneous nanocatalyst in sodium dodecylsulfate micelles. Appl. Organomet. Chem. 2017;31:e3627.

[19] Yazdani E, Miraki MK, Salamatmanesh A, Azarnia J, Azizi K, Ghandi L, Heydari A/A magnetically recoverable copper–salen complex as a nano-catalytic system for amine protection via acetylation using thioacetic acid. Res. Chem. Intermed. 2019;45:1775-1793.

[20] Salamat SA, Younesi H, Bahramifar Faa N/Synthesis of magnetic core–shell Fe_3O_4@TiO_2 nanoparticles from electric arc furnace dust for photocatalytic degradation of steel mill wastewater. RSC Adv. 2017;7:19391-19405.

[21] Zhu J, Li P-Z, Guo W, Zhao Y, Zou R/Titanium-based metal–organic frameworks for photocatalytic applications. Coord. Chem. Rev. 2018;359:80-101.

[22] Tahir MN, Theato P, Oberle P, Melnyk G, Faiss S, Kolb U, Janshoff A, Stepputat M, Tremel W/Facile Synthesis and Characterization of Functionalized, Monocrystalline Rutile TiO_2 Nanorods. Langmuir 2006;22:5209-5212.

[23] Bhagya TC, Krishnan A, Rajan A, Sha MA, Sreelekshmy BR, Jineesh P, Shibli SMA/Exploration and evaluation of proton source-assisted photocatalyst for hydrogen generation. Photochem. Photobiol. Sci. 2019;18:1716-1726.

[24] Dai X, Lu G, Hua Y, Xie X, Wang X, Sun J/Reversible redox behavior of Fe_2O_3/TiO_2 composites in the gaseous photodegradation process. Ceram. Int. 2019;45:13187-13192.

[25] Liu M, Hou SYL, Hu X/Removal of oxytetracycline by Fe_2O_3–TiO_2/modified zeolite composites under visible light irradiation. J. Mater. Sci.: Mater. Electron. 2019;30:9087-9096.

[26] Xu M, Chen Y, Mao G, Zhou B, Low N, Zhang L, Liu Q/TiO_2 Nanoparticle Modified α-Fe_2O_3 Nanospindles For Improved Photoelectrochemical Water Oxidation. Mater. Express 2019;9:133-140.

[27] Chang H, Shang Z, Kong Q, Liu P, Liu J, Luo H/α-Fe_2O_3 nanorods embedded with two-dimensional {0 0 1} facets exposed TiO_2 flakes derived from Ti_3C_2TX MXene for enhanced photoelectrochemical water oxidation. Chem. Eng. J. 2019;370:314-321.

[28] Feng F, Li C, Jian J, Qiao X, Wang H, Jia L/Boosting hematite photoelectrochemical water splitting by decoration of TiO_2 at the grain boundaries. Chem. Eng. J. 2019;368:959-967.

[29] Garcia-Munoz P, Zussblatt NP, Pliego G, Zazo JA, Fresno F, Chmelka BF, Casas JA/Evaluation of photoassisted treatments for norfloxacin removal in water using mesoporous Fe_2O_3-TiO_2 materials. J. Environ. Manage. 2019;238:243-250.

[30] Mendiola-Alvarez SY, Hernández-Ramírez A, Guzmán-Mar JL, Maya-Treviño ML, Caballero-Quintero A, Hinojosa-Reyes L/A novel P-doped Fe_2O_3-TiO_2 mixed oxide: Synthesis, characterization and photocatalytic activity under visible radiation. Catal. Today 2019;328:91-98.

[31] Vigato PA, Tamburini S/The challenge of cyclic and acyclic schiff bases and related derivatives. Coord. Chem. Rev. 2004;248:1717-2128.

[32] Clarke RM, Storr T/ The chemistry and applications of multimetallic salen complexes. Dalton Trans. 2014;43:9380- 9391.

[33] Correia I, Roy S, Matos CP, Borovic S, Butenko N, Cavaco I, Marques F, Lorenzo J, Rodríguez A, Moreno V, Pessoa JC/Vanadium(IV) and copper(II) complexes of

salicylaldimines and aromatic heterocycles: Cytotoxicity, DNA binding and DNA cleavage properties. J. Inorg. Biochem. 2015;147:134-146.

[34] Abd El-Lateef HM, Sayed AR, Adam MSS/Sulfonated salicylidene thiadiazole complexes with Co (II) and Ni (II) ions as sustainable corrosion inhibitors and catalysts for cross coupling reaction. Appl. Organometal. Chem. 2019;33:e4987.

[35] Adam MSS, Mohamad ADM/Catalytic (ep)oxidation and corrosion inhibition potentials of Cu^{II} and Co^{II} pyridinylimino phenolate complexes. Polyhedron 2018;151:118-130.

[36] Kralova K, Kissova K, Švajlenova O, Vanco J/Biological Activity of Copper(II) N-Salicylideneaminoacidato Complexes. Reduction of Chlorophyll Content in Freshwater Alga Chlorella vulgaris and Inhibition of Photosynthetic Electron Transport in Spinach Chloroplasts. Chem. Pap. 2004;58:357-361.

[37] Zehra S, Roisnel T, Arjmand F/Enantiomeric Amino Acid Schiff Base Copper(II) Complexes as a New Class of RNA-Targeted Metallo-Intercalators: Single X-ray Crystal Structural Details, Comparative in Vitro DNA/RNA Binding Profile, Cleavage, and Cytotoxicity. ACS Omega 2019;4:7691-7705.

[38] Reddy PR, Rajeshwar S, Satyanarayana B/ Synthesis, characterization of new copper (ii) Schiff base and 1,10 phenanthroline complexes and study of their bioproperties. Photochem. Photobiol. B 2016;160:217-224.

[39] Vanco J, Švajlenova O, Racanska E, Muselik J, Valentova J/Antiradical activity of different copper(II) Schiff base complexes and their effect on alloxan-induced diabetes. J. Trace Elem. Med. Biol. 2004;18:155-161.

[40] Sun W, Wang Y, Wu X, Yao X/Palladium-, ligand-, and solvent-free synthesis of ynones by the coupling of acyl chlorides and terminal alkynes in the presence of a reusable copper nanoparticle catalyst. Green Chem. 2013;15:2356-2360.

[41] Gawande MB, Goswami A, Felpin F-X, Asefa T, Huang X, Silva R, Zou X, Zbori R, Varma RS/Cu and Cu-Based Nanoparticles: Synthesis and Applications in Catalysis. Chem. Rev. 2016;116:3722-3811.

[42] Cui Y, Qiao L, Li Y, Jing H, Li Y, Wang Q/Synthesis, solid-state structures, and urease inhibition activities of new copper(II) complexes based on O,N,O-tridentate Schiff bases J. Coord. Chem. 2016;69:2318-2328.

[43] Liu X, Manzur C, Novoa N, Celedón S, Carrillo D, Hamon J-R/Multidentate unsymmetrically-substituted Schiff bases and their metal complexes: Synthesis, functional materials properties, and applications to catalysis. Coord. Chem. Rev. 2018;357:144-172.

[44] Chakraborty H, Paul N, Rahman ML/ Catalytic activities of Schiff base aquocomplexes of copper(II) towards hydrolysis of amino acid esters. Transition Met. Chem. 1994;19:524-526.

[45] Saxena P, Murugavel R/Bulky 2,6-dibenzhydryl-4-methylphenyl β-diiminato derived complexes of Pd(II) and Cu(II): Efficient catalysts for Suzuki coupling and alcohol oxidation. J. Organomet. Chem. 2018;868:76-85.

[46] Varyani M, Khatri PK, Jain SL/Amino acid ionic liquid bound copper Schiff base catalyzed highly efficient three component A^3-coupling reaction. Catal. Commun. 2016;77:113-117.

[47] Mureşeanu M, Georgescu I, Bibire LE, Cârjă G/CU^{II}(Sal-Ala)/MgAlLDH and CU^{II}(Sal-Phen)/MgAlLDH as novel catalytic systems for cyclohexene oxidation by H_2O_2. Catal. Commun. 2014;54:39-.

[48] Pratihar JL, Mandal P, Brandão P, Mal D, Felix V/Synthesis, characterization, spectral and catalytic activity of tetradentate (NNNO) azo-imine Schiff base copper(II) complexes. Inorg. Chim. Acta 479 (2018) 221-228.

[49] Shoair AF, El-Shobaky AR, Abo-Yassin HR/Synthesis, spectroscopic characterization, catalytic and antibacterial studies of ruthenium(III) Schiff base complexes. J. Mol. Liq. 2015;211:217-227.

[50] Lehwess-Litzmann A, Neumann P, Parthier C, Ludtke S, Golbik R, Ficner R, Tittmann K/Twisted Schiff base intermediates and substrate locale revise transaldolase mechanism. Nat. Chem. Biol. 2011;7:678-684.

[51] Abdel-Rahman LH, Adam MSS, Abu-Dief AM, Moustafa H, Basha MT, Aboraia AS, Al-Farhan BS, Ahmed HE/Synthesis, theoretical investigations, biocidal screening, DNA binding, in vitro cytotoxicity and molecular docking of novel Cu (II), Pd (II) and Ag (I) complexes of chlorobenzylidene Schiff base: Promising antibiotic and anticancer agents. Appl. Organometal. Chem. 2018;32:e4527.

[52] Adam MSS, Elsawy H/Biological potential of oxo-vanadium salicylediene amino-acid complexes as cytotoxic, antimicrobial, antioxidant and DNA interaction. J. Photochem. Photobio. B 2018;184:34-43.

[53] Al Zoubi W, Al Mohanna N/Membrane sensors based on Schiff bases as chelating ionophores – A review. Spectrochim. Acta A 2014;132:854-870.

[54] Jeevadason AW, Murugavel KK, Neelakantan MA/Review on Schiff bases and their metal complexes as organic photovoltaic materials. Renewable Sustainable Energy Rev. 2014;36:220-227.

[55] Abdel-Rahman LH, Abu-Dief AM, Adam MSS, Hamdan SK/Some New Nano-sized Mononuclear Cu(II) Schiff Base Complexes: Design, Characterization, Molecular Modeling and Catalytic Potentials in Benzyl Alcohol Oxidation. Catal. Lett. 2016;14:1373-1396.

[56] Adam MSS, Hafez AM, El-Ghamry I/Catalytic performance of binary and ternary oxovanadium complexes of dipyridinyl-urea in (ep)oxidation of ***cis***-cyclooctene and 1-octene. Reac. Kinet. Mech. Cat. 2018;124:779-805.

[57] Adam MSS, Abdel-Rahman LH, Abu-Dief AM, Hashem NA/Synthesis, catalysis, antimicrobial activity and DNA interactions of new Cu(II)-Schiff base complexes. Inorg. Nano-Met. Chem. 2020;50:136-150.

[58] Adam MSS/Catalytic potentials of homodioxo-bimetallic dihydrazone complexes of uranium and molybdenum in a homogeneous oxidation of alkenes. Monatsh. Chem. 2015; 146:1823-1836.

[59] Han F-S/Transition-metal-catalyzed Suzuki–Miyaura cross-coupling reactions: a remarkable advance from palladium to nickel catalysts. Chem. Soc. Rev. 2013;42:5270-5298.

[60] Rakhtshah J, Salehzadeh S, Gowdini E, Maleki F, Baghery S, Zolfigol MA/ Synthesis of pyrazole derivatives in the presence of a dioxomolybdenum complex supported on silica-coated magnetite nanoparticles as an efficient and easily recyclable catalyst. RSC Adv. 2016;6:104875-104885.

[61] Hadian-Dehkordi L, Hosseini-Monfared H, Aleshkevych P/A novel chiral manganese-tetraamide macrocycle complex covalently attached to magnetite as recyclable catalyst for aerobic asymmetric epoxidation of olefins. Inorg. Chim. Acta 2017;462:142-151.

[62] Monadi N, Moradi E/A molybdenum(VI) Schiff base complex immobilized on functionalized Fe_3O_4 nanoparticles as a recoverable nanocatalyst for synthesis of 2-amino-4*H*-benzo[*h*]chromenes. Transition Met. Chem. 2018;43:161-170.

[63] Adhikary J, Datta A, Dasgupta S, Chakraborty A, Menendez MI, Chattopadhyay T/Development of an efficient magnetically separable nanocatalyst: theoretical approach on the role of the ligand backbone on epoxidation capability. RSC Adv. 2015;5:92634-92647.

[64] Zheng Y, Duanmu C, Gao Y/A Magnetic Biomimetic Nanocatalyst for Cleaving Phosphoester and Carboxylic Ester Bonds under Mild Conditions. Org. Lett. 2006;8:3215-3217.

[65] Kirar JS, Khare S/Cu(II) Schiff base complex intercalated into layered double hydroxide for selective oxidation of ethylbenzene under solvent-free conditions. RSC Adv. 2018;8:18814-18827.

[66] Rayati S, Abdolalian P/Heterogenization of a molybdenum Schiff base complex as a magnetic nanocatalyst: An eco-friendly, efficient, selective and recyclable nanocatalyst for the oxidation of alkenes. C.R. Chim. 2013;16: 814-820.

[67] Martínez H, Amaya ÁA, Páez-Mozo EA, Martínez FO/Highly efficient epoxidation of α-pinene with O_2 photocatalyzed by dioxoMo(VI) complex anchored on TiO_2 nanotubes. Micropor. Mesopor. Mater. 2018;265:202-210.

[68] Behpour M, Shirazi P, Rahbar M/Immobilization of the Fe2O3/TiO2 photocatalyst on carbon fiber cloth for the degradation of a textile dye under visible light irradiation. Reac. Kinet. Mech. Cat. 2019;127:1073-1085.

[69] Adam MSS, Al-Omair MA, Ullah F/Catalytic comparison of various polar Zn(II)-Schiff base complexes and VO(II)-Schiff base complexes in (ep)oxidation processes of 1,2-cyclohexene and cyclohexane. Res. Chem. Intermediate. 2019;45:4653-4675.

[70] Monfared HH, Bikas R, Mayer P/Homogeneous green catalysts for olefin oxidation by mono oxovanadium(V) complexes of hydrazone Schiff base ligands. Inorg. Chim. Acta 2010;363:2574-2583.

[71] Adam MSS, El-Hady OM, Ullah F/Biological and catalytic potential of sustainable low and high valent metal-Schiff base sulfonate salicylidene pincer complexes. RSC Adv. 2019;9:34311-34329.

[72] Sadeghzadeh SM, Daneshfar F, Malekzadeh M/Manganese(III) Salen Complex Immobilized on Fe_3O_4 Magnetic Nanoparticles: The Efficient, Green and Reusable Nanocatalyst. Chin. J. Chem. 2014;32:349-355.

[73] Eftekhari-Sis B, Akbari M, Amini M, Ashouri F, Bagherzadeh M/Oxoperoxo tungsten(VI) complex immobilized on Schiff base-modified Fe3O4 magnetic nanoparticles as a heterogeneous catalyst for oxidation of alcohols with hydrogen peroxide J. Coord. Chem. 2017;70:328-339

[74] Yuan D, Chen L, Yuan L, Liao S, Yang M, Zhang Q/Superparamagnetic polymer composite microspheres supported Schiff base palladium complex: An efficient and reusable catalyst for the Suzuki coupling reactions. Chem. Eng. J. 2016;287:241-251.

[75] Naghipour A, Fakhri A/Efficient oxidation of sulfides into sulfoxides catalyzed by a chitosan–Schiff base complex of Cu(II) supported on supramagnetic Fe_3O_4 nanoparticles. Environ. Chem. Lett. 2016;14:207-213.

[76] Nemati F, Heravi MM, Elhampoura A/Magnetic nano-Fe_3O_4@TiO_2/Cu_2O core–shell composite: an efficient novel catalyst for the regioselective synthesis of 1,2,3-triazoles using a click reaction. RSC Adv. 2015;5:45775- 45784.

[77] Guo Z, Liu B, Zhang Q, Deng W, Wang Y, Yang Y/Recent advances in heterogeneous selective oxidation catalysis for sustainable chemistry. Chem. Soc. Rev. 2014;43:3480-3524.

[78] Ghabdian M, Nasseri MA, Allahresani A, Motavallizadehkakhky A/ Pd salen complex@CPGO as a convenient, effective heterogeneous catalyst for Suzuki–Miyaura and Heck–Mizoroki cross-coupling reactions. Res. Chem. Intermed. 2018. https://doi.org/10.1007/s11164-018-3455-4.

[79] Kodama RH/Magnetic nanoparticles. J. Magn. Magn. Mater. 1999;200:359-372.

[80] Yin Y, Liu C, Wang B, Yu S, Chen K/The synthesis and properties of bifunctional and intelligent Fe3O4@titanium oxide core/shell nanoparticles. Dalton Trans. 2013;42:7233-7240.

[81] Davari N, Farhadian M, Nazar ARS, Homayoonfal M/ Degradation of diphenhydramine by the photocatalysts of ZnO/Fe_2O_3 and TiO_2/Fe_2O_3 based on clinoptilolite: Structural and operational comparison. J. Environ. Chem. Eng. 2017;5:5707-5720.

[82] Khashan S, Dagher S, Tit N, Alazzam A, Obaidat I/Novel method for synthesis of Fe_3O_4@TiO_2 core/shell nanoparticles. Surf. Coat. Technol. 2017;322:92-98.

[83] Adam MSS/Sustainable dipolar homo-dicopper (II) dihydrazone complex as a catalyst for Sonogashira cross couplings. J. Organomet. Chem. 2019;903:120985.

[84] Noval VE, Carriazo JG/Fe_3O_4-TiO_2 and Fe_3O_4-SiO_2 Core-shell Powders Synthesized from Industrially Processed Magnetite (Fe_3O_4) Microparticles. Mater. Res. 2019;22:e20180660.

[85] Brunauer S, Emmett PH, Teller E/Adsorption of Gases in Multimolecular Layers. J. Am. Chem. Soc. 1938;60:309-319.

[86] Sing KSW/ Adsorption methods for the characterization of porous materials. Adv. Colloid Interfac. Sci. 1998;76–77:3-11.

[87] Zhang Q, Meng G, Wu J, Li D, Liu Z/Study on enhanced photocatalytic activity of magnetically recoverable Fe_3O_4@C@TiO_2 nanocomposites with core–shell nanostructure. Opt. Mater. 2015;46:52-58.

[88] Lee J, Lee Y, Youn JK, Na HN, Yu T, Kim H, Lee S-M, Koo Y-M, Kwak JH, Park HG, Chang HN, Hwang M, Park J-G, Kim J, Hyeonet T/Simple Synthesis of Functionalized Superparamagnetic Magnetite/Silica Core/Shell Nanoparticles and their Application as Magnetically Separable High-Performance Biocatalysts. Small 2008;4:143-152.

[89] Costa AL, Ballarin B, Spegni A, Casoli F, Gardini D/Synthesis of nanostructured magnetic photocatalyst by colloidal approach and spray–drying technique. J. Colloid Interface Sci. 2012;388:31-39.

[90] Liu L, Dong Y, Tang N/A highly efficient and recyclable ligand-free protocol for the Suzuki coupling reaction of potassium aryltrifluoroborates in water. Green Chem. 2014;16:2185-2189.

[91] Ramakrishna V, Reddy ND/Synthesis of zwitterionic palladium complexes and their application as catalysts in cross-coupling reactions of aryl, heteroaryl and benzyl bromides with organoboron reagents in neat water. Dalton Trans. 2017;46:8598-8610.

[92] Mohamad AD, Adam MSS/ Reactivity of base catalysed hydrolysis of 2-pyridinylmethylene-8-quinolinyl-Schiff base iron(II) iodide complexes: solvent effects. Chem. Pap. 2013;67:464-476.

[93] Verma A, Tomar K, Bharadwaj PK/Nanosized Bispyrazole-Based Cryptand-Stabilized Palladium(0) Nanoparticles: A Reusable Heterogeneous Catalyst for the Suzuki–Miyaura Coupling Reaction in Water. Inorg. Chem. 2019;58;1003-1006.

[94] Nakasuka N, Azuma K, Tanaka M/Complex formation of copper(II) acetate with pyridine bases in anhydrous acetic acid. Inorg. Chim. Acta 1995;238:83-87.

[95] Fu Y-F, Song K-P, Zou Z-J, Li M-Q/External cross-linked sulfonate-functionalized ***N***-heterocyclic carbenes: an efficient and recyclable catalyst for Suzuki–Miyaura reactions in water. Transition Met. Chem. 2018;43:665-672.

[96] S. Fortun, P. Beauclair, A.R. Schmitzer/Metformin as a versatile ligand for recyclable palladium-catalyzed cross-coupling reactions in neat water. RSC Adv. 2017;7:21036-21044.

[97] McGivern WS, Derecskei-Kovacs A, North SW, Francisco JS/Computationally Efficient Methodology to Calculate C−H and C−X (X = F, Cl, and Br) Bond Dissociation Energies in Haloalkanes. J. Phys. Chem. A 2000;104:436-442.

[98] Boruah PR, Gehlot PS, Kumar A, Sarma D/Palladium immobilized on the surface of MMT K 10 with the aid of [BMIM][BF_4]: An efficient catalyst for Suzuki-Miyaura cross-coupling reactions. Mol. Catal. 2018;461:54-59.

[99] Heidari B, Heravi MM, Nabid MR, Sedghi R, Hooshmand SE/Novel palladium nanoparticles supported on β-cyclodextrin@graphene oxide as magnetically recyclable catalyst for Suzuki–Miyaura cross-coupling reaction with two different approaches in bio-based solvents. Appl. Organometal. Chem. 2019;33:e4632.

[100] Azad M, Rostamizadeh S, Nouri F, Estiri H, Fadakar Y/Pd nanoparticles at N-heterocyclic carbene at ZIF-8 as an ultrafine, robust and sustainable heterogeneous system for Suzuki-Miyaura cross coupling processes. Mat. Lett. 2019;236:757-760.

[101] Nasrollahzadeh M, Sajjadi M, Khonakdar HA/Synthesis and characterization of novel Cu(II) complex coated Fe_3O_4@SiO_2 nanoparticles for catalytic performance. J. Mol. Struct. 2018;1161:453-463.

Figures captions

Figure 1: UV-Vis. absorption spectroscopy of HL and its Cu(II)-complex (CuL).

Figure 2: FT-IR spectra of CuL, Fe_3O_4, TiO_2@Fe_3O_4 and CuL@TiO_2@Fe_3O_4.

Figure 3: FE-SEM and Energy-dispersive X-ray spectroscopy (EDS) analyses of (a) Fe_3O_4 nanoparticles, (b) TiO_2@Fe_3O_4, and (c) CuL@TiO_2@Fe_3O_4.

Figure 4: HR-TEM images of (a) Fe_3O_4 nanoparticles, (b) TiO_2@Fe_3O_4 and (c) CuL@TiO_2@Fe_3O_4.

Figure 5: X-ray diffraction pattern of (a) Fe_3O_4 nanoparticles, (b) TiO_2@Fe_3O_4 and (c) CuL@TiO_2@Fe_3O_4.

Figure 6: Magnetization vs. applied field of Fe_3O_4, TiO_2@Fe_3O_4 and CuL@TiO_2@Fe_3O_4.

Figure 7: TGA of CuL and CuL@TiO_2@Fe_3O_4.

Figure 8: Nitrogen adsorption-desorption isotherms of CuL@TiO_2@Fe_3O_4.

Figure 9: BET surface area plot of CuL@TiO_2@Fe_3O_4 sample.

Figure 10: The yield percentages of C—C biaryl products for (a) phenylboronic acid and 2-pyridyl bromide coupling (Suzuki-Miyaura reaction); (b) 2-aminopyridine and 2-pyridyl bromide coupling (Buchwald-Hartewig reaction) catalyzed by CuL and CuL@TiO_2@Fe_3O_4 in toluene, with presence of K_2CO_3, as a function of time at 100 °C.

Figure 11: The number of reusability of CuL and CuL@TiO_2@Fe_3O_4 in the Suzuki-Miyaura cross-coupling reaction of phenylboronic acid and 2-pyridyl bromide in presence of K_2CO_3 and in ethanol at 100 °C.

Figure 12: Energy-dispersive X-ray spectroscopy (EDS) of the reused seven times CuL@TiO_2@Fe_3O_4 heterostructure as a heterogeneous catalyst for Suzuki-Miyaura reactions of phenylboronic acid with 2-pyridyl bromide in presence of K_2CO_3 and in ethanol at 100 °C.

Table captions

Table 1: Significant C, H and N analyses and melting point (m.p.) of HL and CuL. Magnetic moments, μ_{eff}, and electronic spectral transitions of HL and CuL at [HL] = [CuL] = 1×10^{-5} mol dm^{-3} in methanol and 25 °C.

Table 2: Suzuki-Miyaura C—C reaction of phenylboronic acid with 2-pyridyl halide catalyzed by CuL or CuL@TiO_2@Fe_3O_4 under various conditions.

Table 3: Buchwald-Hartwig C—N reaction of 2-aminopyridine with pyridyl halide catalyzed by CuL or CuL@TiO_2@Fe_3O_4 under various conditions.

Table 4: Suzuki-Miyaura C—C reaction of phenylboronic acid with 2-pyridyl bromide catalyzed by Fe_3O_4, TiO_2@Fe_3O_4 or CuL@TiO_2@Fe_3O_4 under the optimized reaction conditions.

Table 5: Effect of loaded amount of CuL or CuL@TiO_2@Fe_3O_4 on the Buchwald-Hartwig C—C reactions of phenylboronic acid with 2-pyridyl bromide under the optimized conditions.

List of Tables

Table 1

Significant C, H and N analyses and melting point (m.p.) of HL and CuL. Magnetic moments, μ_{eff}, and electronic spectral transitions of HL and CuL at [HL] = [CuL] = 1×10^{-5} mol dm^{-3} in methanol and 25 °C.

Comp.	MW (g mol^{-1})	Microanalyses found %, (calc. %)			m.p. (°C)	Appearance	Electronic Spectra			μ_{eff} (B.M.)
		C	H	N			λ_{max} (nm)	ε_{max} (mol^{-1} cm^{-1})	Assign.	
HL	236.27	60.66 (61.00)	6.52 (6.83)	12.23 (11.86)	54	Orange red	352 321	6054 6149	L-CT n→π*	--
CuL	370.72	38.78 (38.88)	4.13 (4.35)	7.67 (7.56)	211	Green	647 301	4107 5213	d—d n→π*	2.93

Table 2

Suzuki-Miyaura C—C reaction of phenylboronic acid with 2-pyridyl halide catalyzed by CuL or CuL@TiO_2@Fe_3O_4 under various conditions.

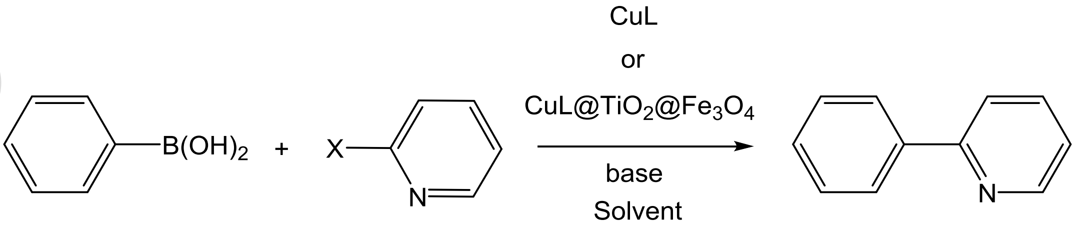

Entry[a]	Phenylbronic acid	Pyridyl halide	Catalyst	Base	Solvent	Yield, %[b]
1	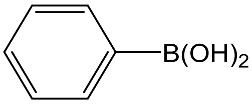	Br—	--	K_2CO_3	Toluene	16
2		Br—	CuL	--	Toluene	28
3		Br—	CuL	K_2CO_3	Toluene	82
4		Cl—	CuL	K_2CO_3	Toluene	75
5		Br—	CuL@TiO_2@Fe_3O_4	K_2CO_3	Toluene	90
6		Cl—	CuL@TiO_2@Fe_3O_4	K_2CO_3	Toluene	81
7		Br—	CuL	*t*BuOK	Toluene	65
8		Br—	CuL	K_3PO_4	Toluene	53
9		Br—	CuL@TiO_2@Fe_3O_4	*t*BuOK	Toluene	72
10		Br—	CuL@TiO_2@Fe_3O_4	K_3PO_4	Toluene	66
11		Br—	CuL	KOH	Toluene	37
12		Br—	CuL@TiO_2@Fe_3O_4	KOH	Toluene	44
13		Br—	CuL	K_2CO_3	$CHCl_3$	88
14		Cl—	CuL	K_2CO_3	$CHCl_3$	84
15		Br—	CuL@TiO_2@Fe_3O_4	K_2CO_3	$CHCl_3$	89
16		Cl—	CuL@TiO_2@Fe_3O_4	K_2CO_3	$CHCl_3$	80
17		Br—	CuL	K_2CO_3	H_2O	71
18		Cl—	CuL	K_2CO_3	H_2O	57
19		Br—	CuL@TiO_2@Fe_3O_4	K_2CO_3	H_2O	75
20		Cl—	CuL@TiO_2@Fe_3O_4	K_2CO_3	H_2O	62
21		Br—	CuL	*t*BuOK	H_2O	62
22		Br—	CuL	K_3PO_4	H_2O	55
23		Br—	CuL@TiO_2@Fe_3O_4	*t*BuOK	H_2O	59
24		Br—	CuL@TiO_2@Fe_3O_4	K_3PO_4	H_2O	51
25		Br—	CuL	K_2CO_3	EtOH	89
26		Cl—	CuL	K_2CO_3	EtOH	83
27		Br—	CuL@TiO_2@Fe_3O_4	K_2CO_3	EtOH	91
28		Cl—	CuL@TiO_2@Fe_3O_4	K_2CO_3	EtOH	85
29		Br—	CuL	*t*BuOK	EtOH	76
30		Br—	CuL	K_3PO_4	EtOH	81

31	Br—	CuL@TiO_2@Fe_3O_4	*t*BuOK	EtOH	80
32	Br—	CuL@TiO_2@Fe_3O_4	K_3PO_4	EtOH	79
33	Br—	CuL	K_2CO_3	EtOH:H_2O (1:1)	79
34	Cl—	CuL	K_2CO_3	EtOH:H_2O (1:1)	72
35	Br—	CuL@TiO_2@Fe_3O_4	K_2CO_3	EtOH:H_2O (1:1)	87
36	Cl—	CuL@TiO_2@Fe_3O_4	K_2CO_3	EtOH:H_2O (1:1)	75
37	Br—	CuL	*t*BuOK	EtOH:H_2O (1:1)	70
38	Br—	CuL	K_3PO_4	EtOH:H_2O (1:1)	64
39	Br—	CuL@TiO_2@Fe_3O_4	*t*BuOK	EtOH:H_2O (1:1)	72
40	Br—	CuL@TiO_2@Fe_3O_4	K_3PO_4	EtOH:H_2O (1:1)	70

[a] Phenylboronic acid (1.0 mmol), pyridyl halide (1.1 mmol), base (2.0 mmol), solvent (10 mL) and catalyst (CuL, 0.02 mmol, CuL@TiO_2@Fe_3O_4, 0.20 g) at 100 °C after 4 h for CuL and 6 h for CuL@TiO_2@Fe_3O_4.

[b] The yield percentages of the C—C product was detected by GC-MS.

Table 3

Buchwald-Hartwig C—N reaction of 2-aminopyridine with pyridyl halide catalyzed by CuL or CuL@TiO_2@Fe_3O_4 under various conditions.

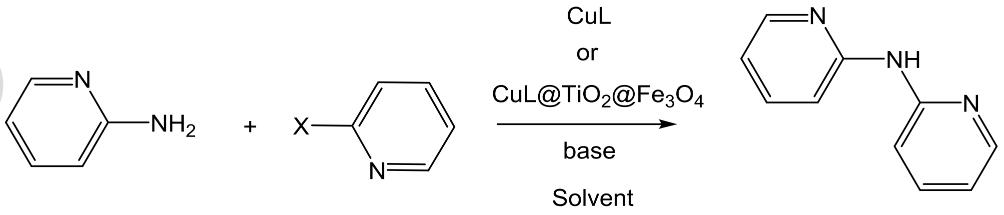

Entry[a]	2-Aminopyridine	Pyridyl halide	Catalyst	Base	Solvent	Yield, %[b]
1	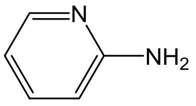	Br—	CuL	K_2CO_3	Toluene	88
2		Cl—	CuL	K_2CO_3	Toluene	84
3		Br—	CuL@TiO_2@Fe_3O_4	K_2CO_3	Toluene	92
4		Cl—	CuL@TiO_2@Fe_3O_4	K_2CO_3	Toluene	87
5		Br—	CuL	*t*BuOK	Toluene	76
6		Br—	CuL	K_3PO_4	Toluene	69
7		Br—	CuL@TiO_2@Fe_3O_4	*t*BuOK	Toluene	77
8		Br—	CuL@TiO_2@Fe_3O_4	K_3PO_4	Toluene	75
9		Br—	CuL	KOH	Toluene	42
10		Br—	CuL@TiO_2@Fe_3O_4	KOH	Toluene	49
11		Br—	CuL	K_2CO_3	$CHCl_3$	91
12		Cl—	CuL	K_2CO_3	$CHCl_3$	87
13		Br—	CuL@TiO_2@Fe_3O_4	K_2CO_3	$CHCl_3$	92
14		Cl—	CuL@TiO_2@Fe_3O_4	K_2CO_3	$CHCl_3$	88
15		Br—	CuL	K_2CO_3	H_2O	68
16		Cl—	CuL	K_2CO_3	H_2O	65
17		Br—	CuL@TiO_2@Fe_3O_4	K_2CO_3	H_2O	71
18		Cl—	CuL@TiO_2@Fe_3O_4	K_2CO_3	H_2O	67
19		Br—	CuL	*t*BuOK	H_2O	63
20		Br—	CuL	K_3PO_4	H_2O	55
21		Br—	CuL@TiO_2@Fe_3O_4	*t*BuOK	H_2O	62
22		Br—	CuL@TiO_2@Fe_3O_4	K_3PO_4	H_2O	59
23		Br—	CuL	K_2CO_3	EtOH	91
24		Cl—	CuL	K_2CO_3	EtOH	88
25		Br—	CuL@TiO_2@Fe_3O_4	K_2CO_3	EtOH	94
26		Cl—	CuL@TiO_2@Fe_3O_4	K_2CO_3	EtOH	87
27		Br—	CuL	*t*BuOK	EtOH	83
28		Br—	CuL	K_3PO_4	EtOH	75
29		Br—	CuL@TiO_2@Fe_3O_4	*t*BuOK	EtOH	84
30		Br—	CuL@TiO_2@Fe_3O_4	K_3PO_4	EtOH	72

31	Br—	CuL	K_2CO_3	$EtOH:H_2O$ (1:1)	78
32	Cl—	CuL	K_2CO_3	$EtOH:H_2O$ (1:1)	76
33	Br—	$CuL@TiO_2@Fe_3O_4$	K_2CO_3	$EtOH:H_2O$ (1:1)	81
34	Cl—	$CuL@TiO_2@Fe_3O_4$	K_2CO_3	$EtOH:H_2O$ (1:1)	77
35	Br—	CuL	*t*BuOK	$EtOH:H_2O$ (1:1)	75
36	Br—	CuL	K_3PO_4	$EtOH:H_2O$ (1:1)	70
37	Br—	$CuL@TiO_2@Fe_3O_4$	*t*BuOK	$EtOH:H_2O$ (1:1)	78
38	Br—	$CuL@TiO_2@Fe_3O_4$	K_3PO_4	$EtOH:H_2O$ (1:1)	74

[a] 2-Aminopyridine (1.0 mmol), pyridyl halide (1.1 mmol), base (2.0 mmol), solvent (10 mL) and catalyst (0.20 g) at 100 °C after 3 h for CuL and 4 h for $CuL@TiO_2@Fe_3O_4$.

[b] The yield percentages of the C—N product was detected by GC-MS.

Table 4

Suzuki-Miyaura C—C reaction of phenylboronic acid with 2-pyridyl bromide catalyzed by Fe_3O_4, $TiO_2@Fe_3O_4$ or $CuL@TiO_2@Fe_3O_4$ under the optimized reaction conditions.

Entry[a]	Catalyst	Yield, %[b]
1	Fe_3O_4	71
2	$TiO_2@Fe_3O_4$	83
3	$CuL@TiO_2@Fe_3O_4$	91

[a] Phenylboronic acid (1.0 mmol), 2-pyridyl bromide (1.1 mmol), base (2.0 mmol), ethanol (10 mL) and catalyst (0.02 g) at 100 °C after 6 h.

[b] The yield percentages of the C—C product was detected by GC-MS.

Table 5

Effect of loaded amount of CuL or CuL@TiO_2@Fe_3O_4 on the Buchwald-Hartwig C—C reactions of phenylboronic acid with 2-pyridyl bromide under the optimized conditions.

Entry[a]	Catalyst	Amount	Yield, %[b]
1	CuL	0.01 mmol	78
2		0.02 mmol	89
3		0.05 mmol	89
4		0.10 mmol	81
5	CuL@TiO_2@Fe_3O_4	0.05 g	73
6		0.1 g	90
7		0.2 g	91
8		0.5 g	89

[a] Phenylboronic acid (1.0 mmol), 2-pyridyl bromide (1.1 mmol), K_2CO_3 (2.0 mmol), ethanol (10 mL) and catalyst at 100 °C after 4 h for CuL and 6 h for CuL@TiO_2@Fe_3O_4.

[b] The yield percentages of the C—C product was detected by GC-MS.

Table 6

Suzuki-Miyaura C—C reaction of phenylboronic acid with various heterocyclic bromides catalyzed by CuL or CuL@TiO_2@Fe_3O_4 under optimized conditions.

Entry[a]	Phenylbronic acid	heterocyclic bromides	Product	Catalyst	Yield, %[b]
1	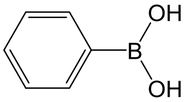	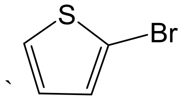	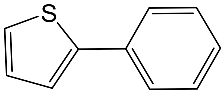	CuL	60
2				CuL@TiO_2@Fe_3O_4	67
3		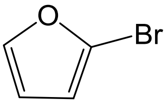	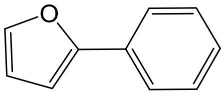	CuL	61
4				CuL@TiO_2@Fe_3O_4	70
5		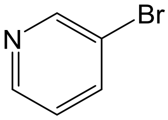	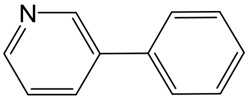	CuL	72
6				CuL@TiO_2@Fe_3O_4	79
7		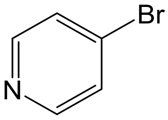	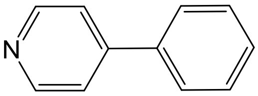	CuL	71
8				CuL@TiO_2@Fe_3O_4	77
9		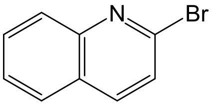	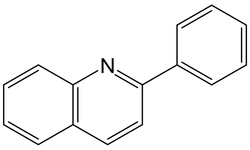	CuL	76
10				CuL@TiO_2@Fe_3O_4	71
11		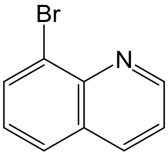	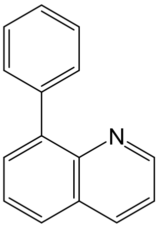	CuL	75
12				CuL@TiO_2@Fe_3O_4	68

[a] Phenylbronic acid (1.0 mmol), heterocyclic bromides (1.1 mmol), K_2CO_3 (2.0 mmol), ethanol (10 mL) and catalyst (0.20 g) at 100 °C after 3 h for CuL and 4 h for CuL@TiO_2@Fe_3O_4.

[b] The yield percentages of the C—C product was detected by GC-MS.

Table 7

Buchwald-Hartwig C—N reaction of 2-aminopyridine with various heterocyclic bromides catalyzed by CuL or CuL@TiO_2@Fe_3O_4 under the optimized conditions.

Entry[a]	Phenylbronic acid	heterocyclic bromides	Product	Catalyst	Yield, %[b]
1	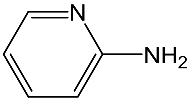	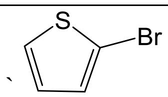	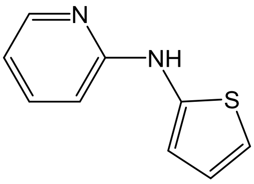	CuL	53
2				CuL@TiO_2@Fe_3O_4	64

This article is protected by copyright. All rights reserved

3	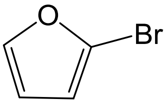	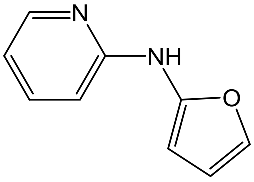	CuL	58
4			CuL@TiO$_2$@Fe$_3$O$_4$	72
5	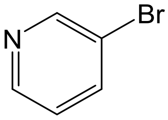	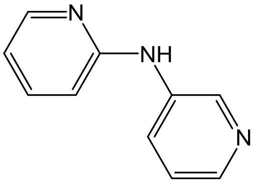	CuL	72
6			CuL@TiO$_2$@Fe$_3$O$_4$	81
7	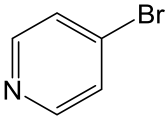	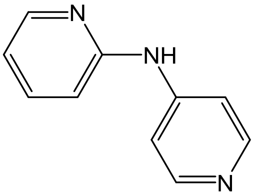	CuL	74
8			CuL@TiO$_2$@Fe$_3$O$_4$	80
9	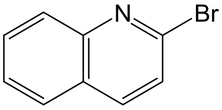	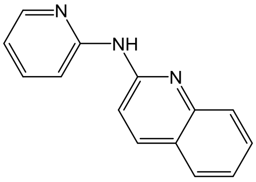	CuL	78
10			CuL@TiO$_2$@Fe$_3$O$_4$	79
11	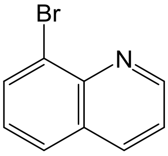	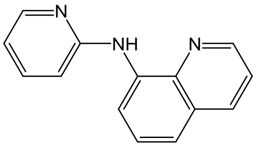	CuL	82
12			CuL@TiO$_2$@Fe$_3$O$_4$	87

---

[a] 2-Aminopyridine (1.0 mmol), heterocyclic bromides (1.1 mmol), K$_2$CO$_3$ (2.0 mmol), ethanol (10 mL) and catalyst (0.20 g) at 100 °C after 3 h for CuL and 4 h for CuL@TiO$_2$@Fe$_3$O$_4$.

[b] The yield percentages of the C—N product was detected by GC-MS.

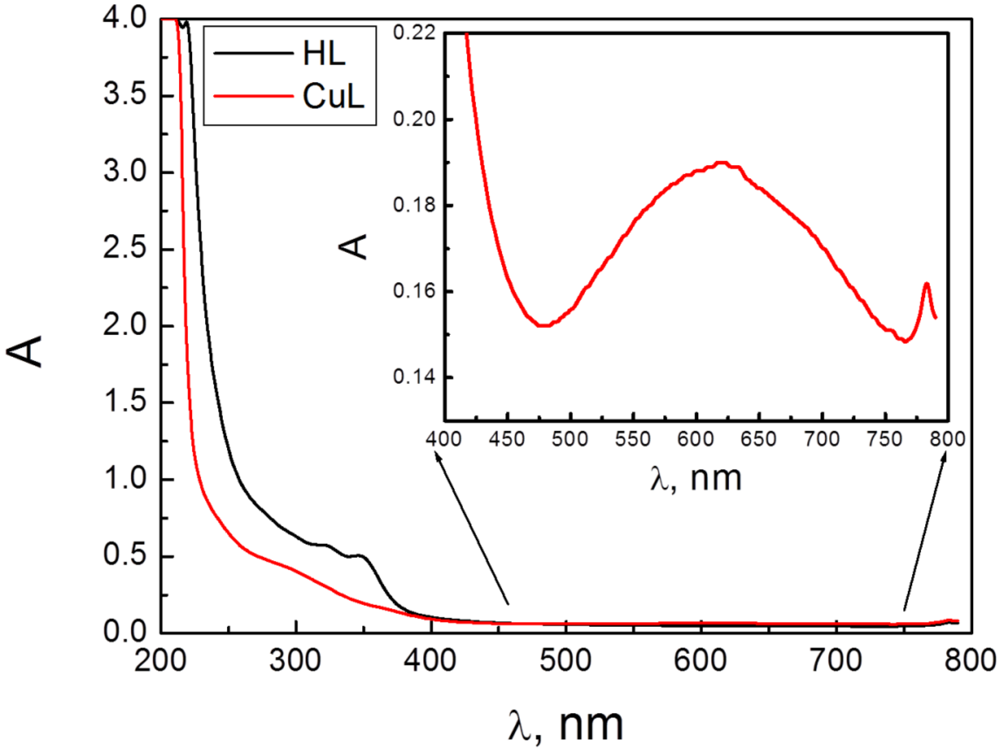

jace_17098_f1.tif

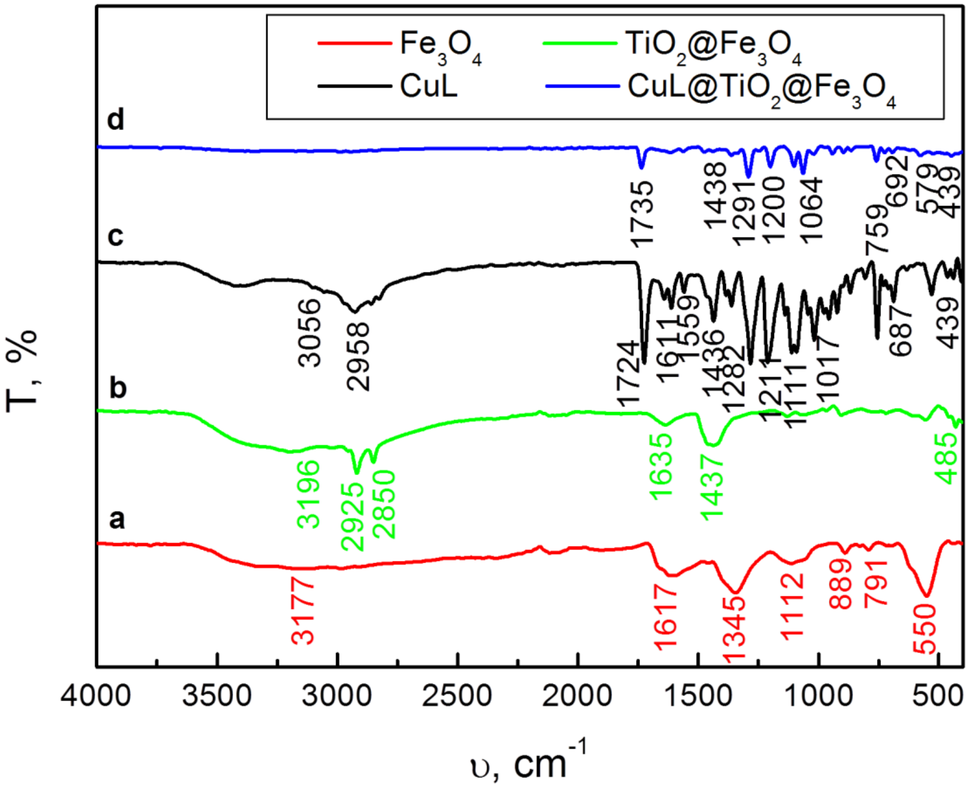

jace_17098_f2.tif

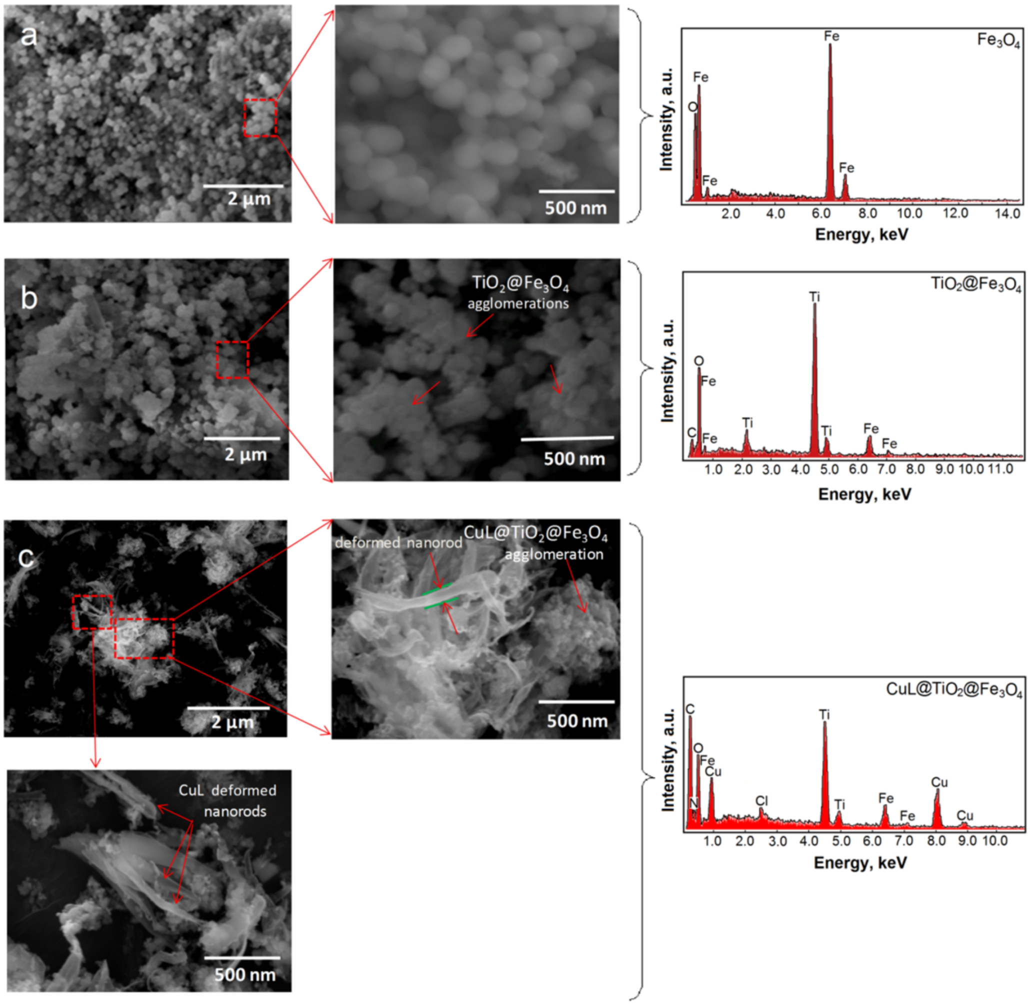

jace_17098_f3.tif

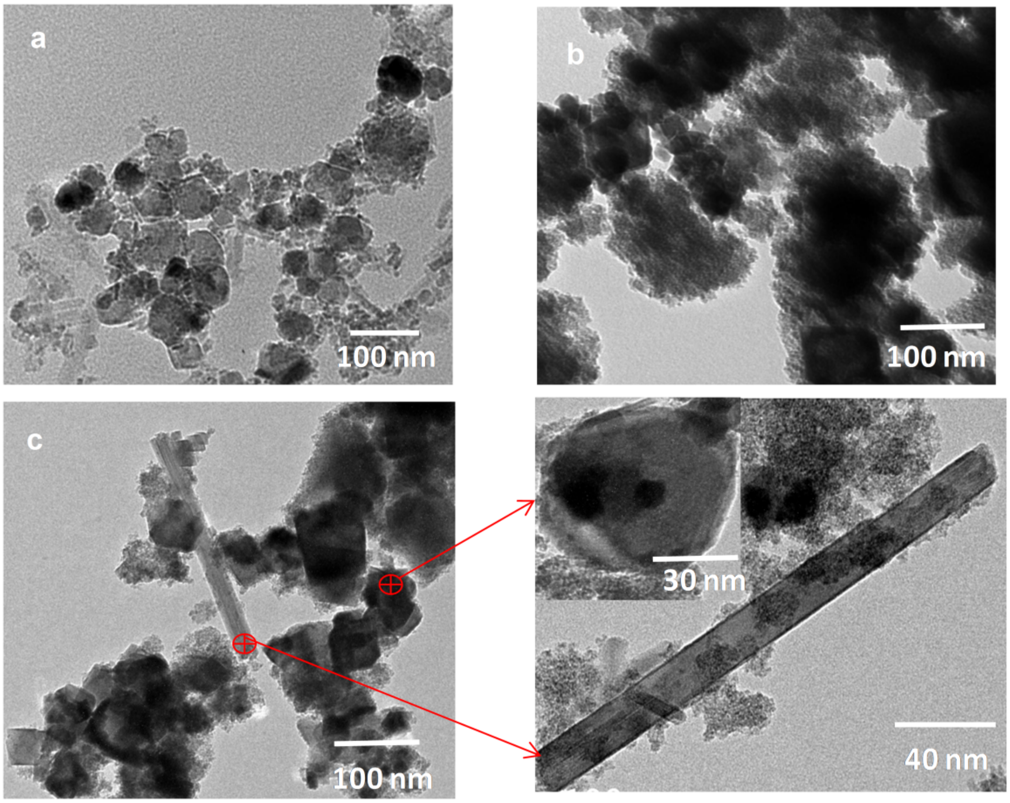

jace_17098_f4.tif

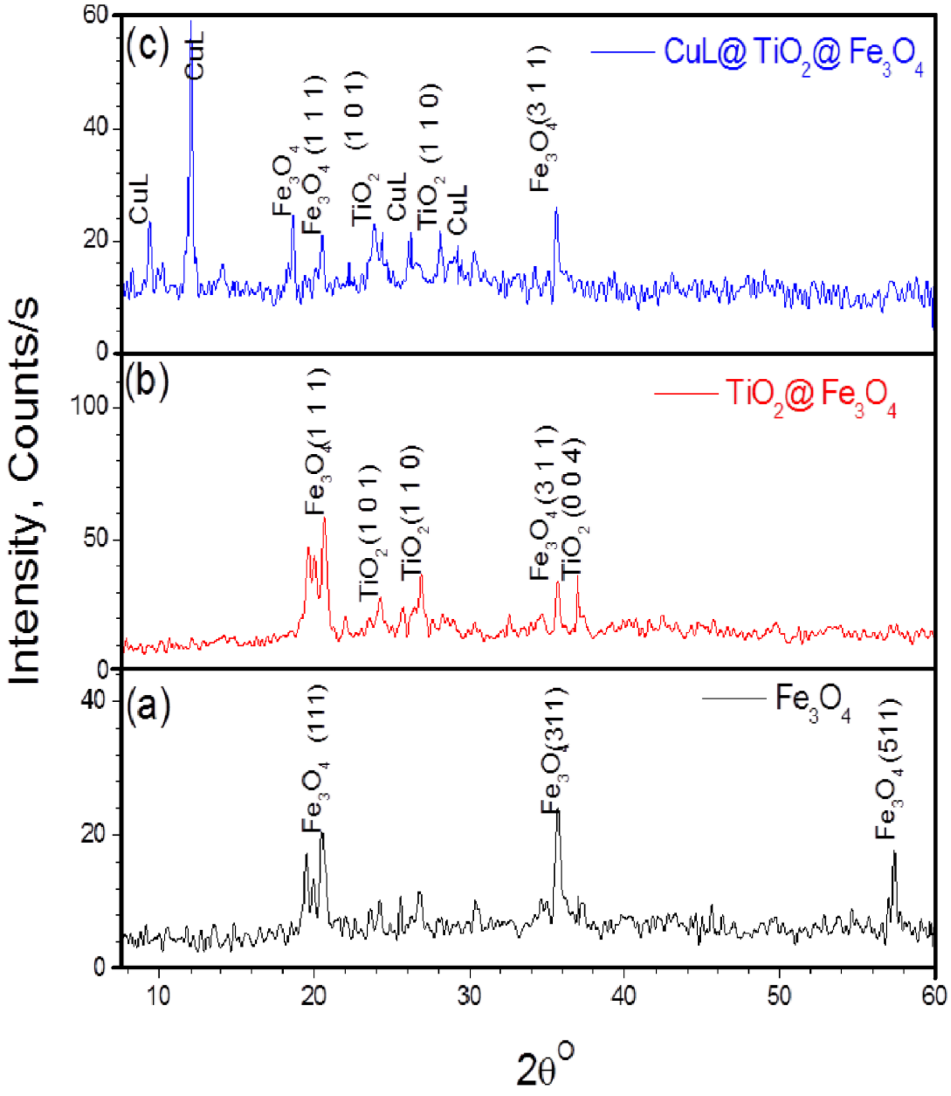

jace_17098_f5.tif

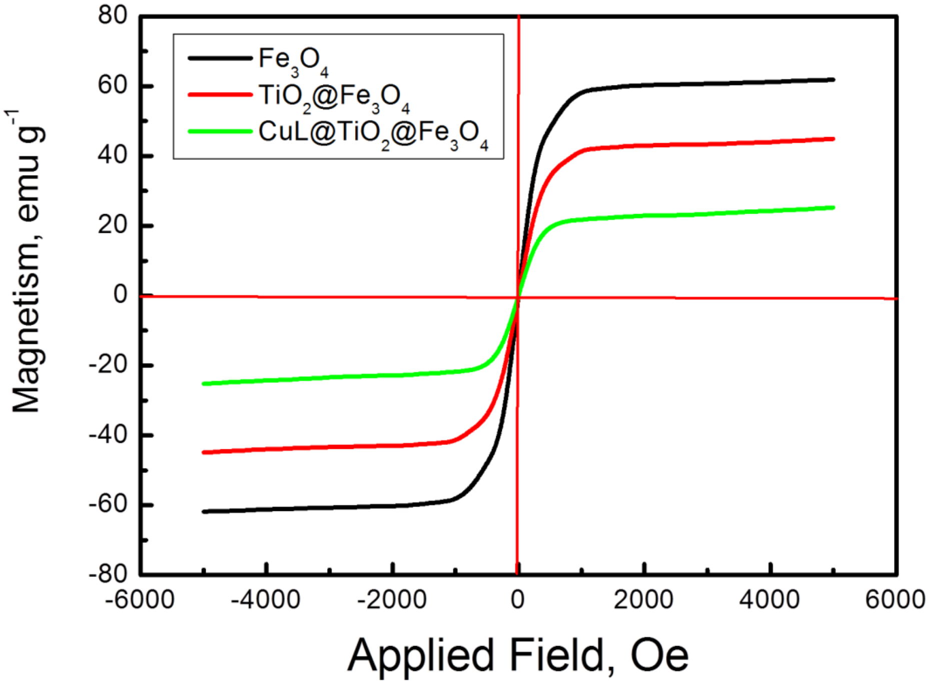

jace_17098_f6.tif

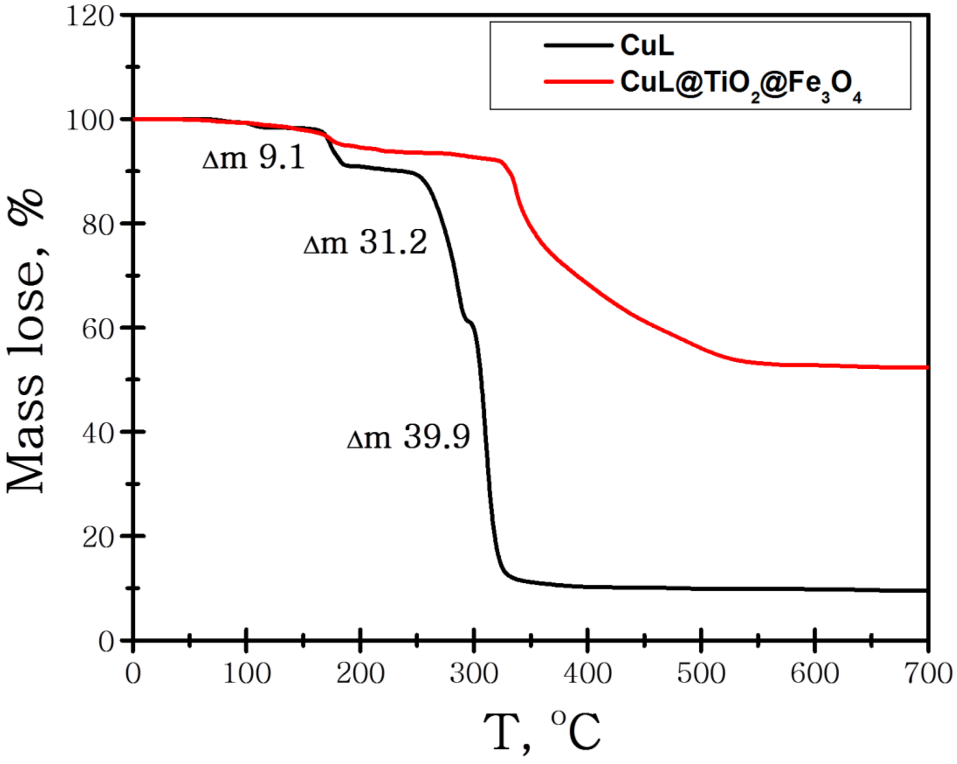

jace_17098_f7.tif

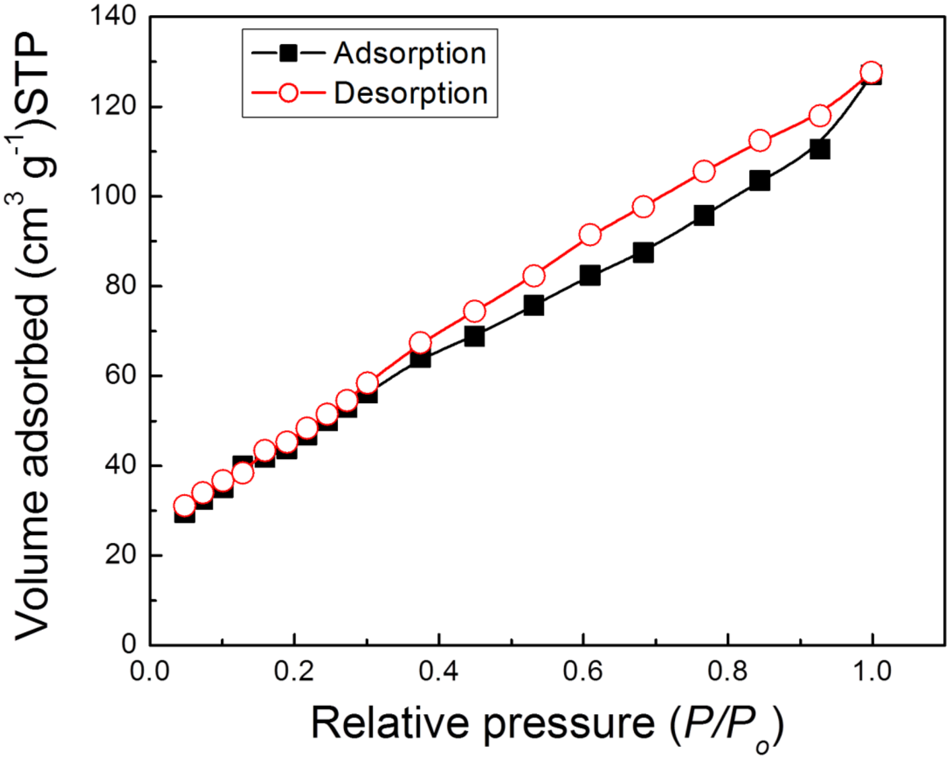

jace_17098_f8.tif

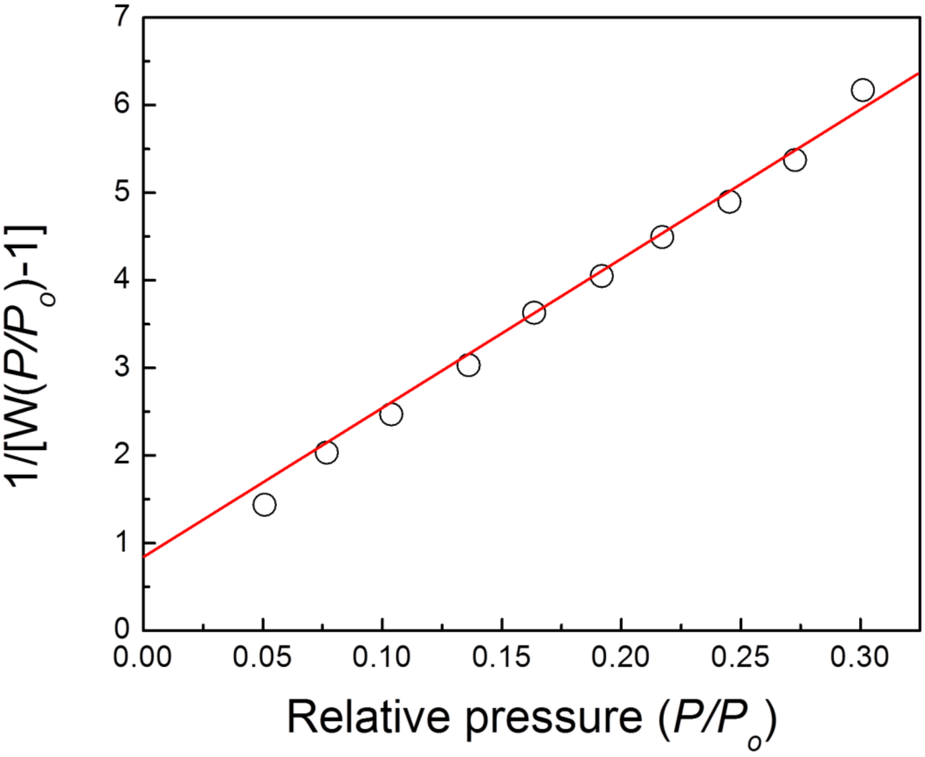

jace_17098_f9.tif

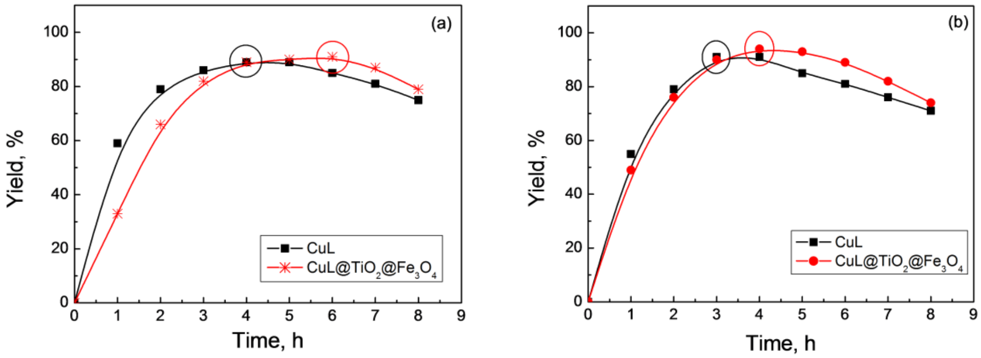

jace_17098_f10.tif

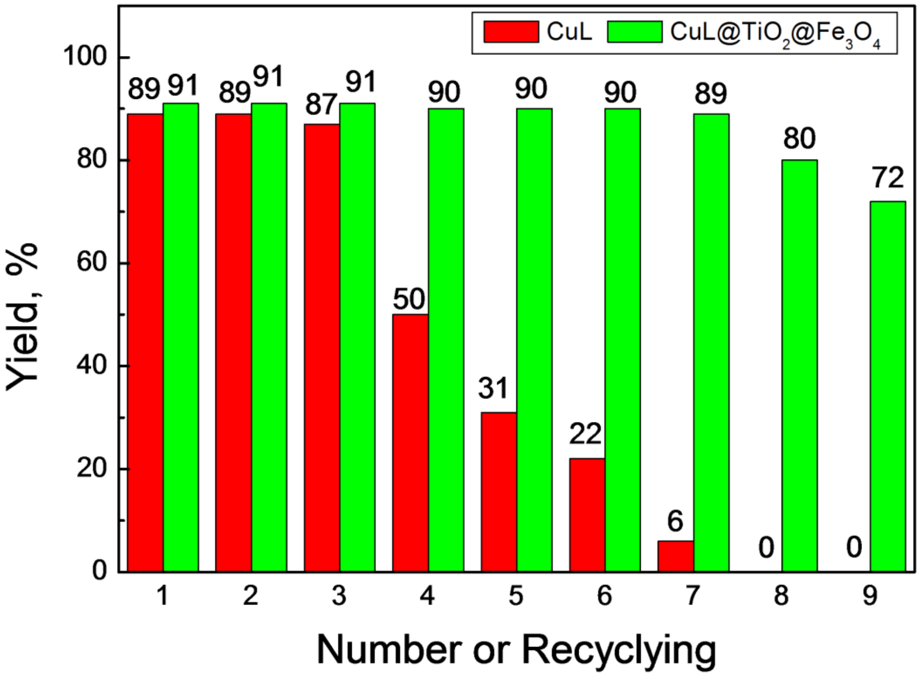

jace_17098_f11.tif

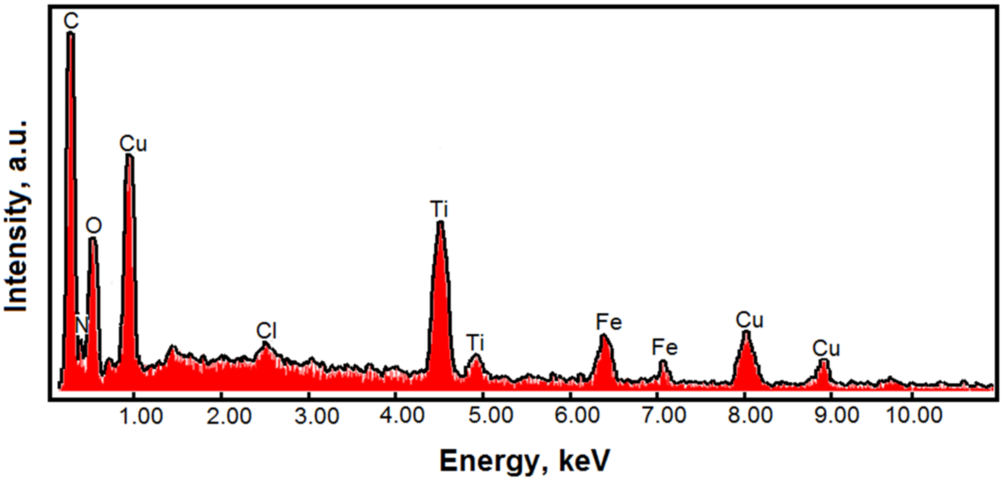

jace_17098_f12.tif